Eur Biophys J (2014) 43:517–544
DOI 10.1007/s00249-014-0982-9

ORIGINAL PAPER

EBSA
Biophysics in Europe

Effect of the cosolutes trehalose and methanol on the equilibrium and phase-transition properties of glycerol-monopalmitate lipid bilayers investigated using molecular dynamics simulations

Monika Laner · Bruno A. C. Horta · Philippe H. Hünenberger

Received: 19 May 2014 / Revised: 16 July 2014 / Accepted: 24 July 2014 / Published online: 24 August 2014

Abstract The influence of the cosolutes trehalose and methanol on the structural, dynamic and thermodynamic properties of a glycerol-1-monopalmitate (GMP) bilayer and on its main transition temperature T_m is investigated using atomistic molecular dynamics simulations (600 ns) of a GMP bilayer patch ($2 \times 8 \times 8$ lipids) at different temperatures in the range of 302 to 338 K and considering three different cosolute concentrations. Depending on the environment and temperature, these simulations present no or a single GL→LC, LC→GL or LC→ID transition, where LC, GL and ID are the liquid crystal, gel and interdigitated phases, respectively. The trehalose molecules form a coating layer at the bilayer surface, promote the hydrogen-bonded bridging of the lipid headgroups, preserve the interaction of the headgroups with trapped water and induce a slight lateral expansion of the bilayer in the LC phase, observations that may have implications for the phenomenon of anhydrobiosis. However, this cosolute does not affect T_m and its dependence on hydration in the concentration range considered. On the other hand, methanol molecules intercalate between the lipid headgroups, promote a lateral expansion of the bilayer in the LC phase and induce a concentration dependent decrease of T_m, observations that may have implications for the phenomenon of anesthesia. The occurrence of an ID phase in the presence of this cosolute may be viewed as an extreme consequence of lateral expansion. The analysis of the simulations also suggests the existence of two basic conservation principles: (1) the hydrogen-bond saturation principle rests on the observation that for all species present in the different systems, the total numbers of hydrogen-bonds per molecule is essentially constant, the only factor of variability being their distribution among different partners; (2) the densest packing principle rests on the observation that the effective volume per methylene group in the interior of the bilayer is only weakly sensitive to the environment, with values comparable to those for liquid (LC) and solid (ID) alkanes, or intermediate (GL).

Keywords Molecular dynamics · Lipid bilayer · Monoglyceride · Glycerol monopalmitate · Phase transition · Trehalose · Methanol

Electronic supplementary material The online version of this article (doi:10.1007/s00249-014-0982-9) contains supplementary material, which is available to authorized users.

M. Laner · B. A. C. Horta · P. H. Hünenberger
Laboratory of Physical Chemistry, ETH Zürich, Zurich, Switzerland

B. A. C. Horta
Dpto. de Engenharia Elétrica, PUC-Rio, Rio de Janeiro, Brazil

B. A. C. Horta
Dpto. de Ciências Biológicas, UEZO, Rio de Janeiro, Brazil

P. H. Hünenberger (✉)
Laboratory of Physical Chemistry, ETH Hönggerberg, HCI, 8093 Zurich, Switzerland
e-mail: phil@igc.phys.chem.ethz.ch

Introduction

Lipid bilayers, the main constituents of biological membranes, are of crucial importance to all living organisms because they represent the boundaries defining the different cellular compartments and the barrier to the extracellular medium, as well as the first interaction site of the cell with this medium (Cooper and Hausman 2007).

Aqueous lipid systems can present many different phases (Foubert et al. 2007), depending on the types of the

lipid molecules, on their concentrations, and on the possible presence of cosolutes (CSLs). The two biologically most relevant of these phases are bilayer phases, namely the gel (GL) and the liquid crystal (LC) phases (Seddon and Cevc 1993). In the GL phase, the aliphatic lipid tails are arranged in nearly all-*trans* conformations and in orientations that are generally tilted with respect to the bilayer normal. In the LC phase, the tails are disordered, presenting a mixture of *trans* and *gauche* conformations, and no preferential orientation of the chains (collective tilting) is observed. Compared to the GL phase, the LC phase is also laterally more expanded and transversely more compact. For a given bilayer composition and under specified environmental conditions (pressure, hydration level, nature and concentration of possible CSLs), the temperature at which the GL↔LC transition occurs is called the main transition (or melting) temperature T_m. Understanding the influence of composition and environment on this temperature, as well as on the properties of the two phases, is of fundamental biological and technological importance (Seddon and Cevc 1993; Nagle and Tristram-Nagle 2000).

There are three basic mechanisms whereby the mechanical and permeability properties of the cell membrane can be modulated by CSLs present in the intra- or extra-cellular medium: (1) direct interaction of the CSL molecules with specific membrane-bound proteins, such as ion or water channels (Pierce et al. 2002; Hicke and Dunn 2003; Kristiansen 2004); (2) direct alteration of the phase properties (structure, fluidity, melting temperature) of the bilayer induced by lipid-CSL interactions (Crowe et al. 1987; Lee et al. 2004; Chanda and Bandyopadhyay 2006; Yamamoto et al. 2012); (3) indirect modulation of the properties of membrane-bound proteins via an alteration of the bilayer phase properties (Barchfeld and Deamer 1988; Cantor 2001; Rudolph and Antkowiak 2004; Franks 2006). While the first type of mechanism implies the existence of a specific protein receptor for the CSL, the two others rely on a generic form of lipid-CSL interaction. Important mechanisms of the second and third types are responsible, respectively, for the phenomena of anhydrobiosis in the presence of, e.g., sugars (Keilin 1959; Crowe et al. 1987; Wright 2001; Clegg 2001; Feovilova 2003) and of anesthesia in the presence of, e.g., xenon (Yamamoto et al. 2012), alcohols (Chanda and Bandyopadhyay 2006; MacCallum and Tieleman 2008), or other small molecules (MacCallum and Tieleman 2008).

The phenomenon of anhydrobiosis (Crowe et al. 1992, 1998, 2002; Sun et al. 1997; Hoekstra et al. 2001; Hincha et al. 2002; Tunnacliffe and Lapinski 2003; Hincha and Hagemann 2004; Watanabe 2006; Adams et al. 2007) corresponds to a reversible suspension of life under conditions of extreme dehydration. In the absence of CSL, dehydration of a lipid bilayer typically promotes an increase in its melting temperature (Krog and Larsson 1968; Crowe et al. 1987). In organisms undergoing a dehydration stress, portions of the cell membrane would therefore undergo a LC→GL transition, resulting in membrane disruption upon rehydration. In anhydrobiotic organisms, such a transition is prevented by the accumulation of specific CSLs in the intracellular medium, in particular sugars, and most prominently the disaccharide trehalose (Crowe et al. 1984, 1992, 2005; Green and Angell 1989; Belton and Gil 1994; Koster et al. 1994; Guppy and Withers 1999; Tunnacliffe et al. 2001; Clegg 2001; Crowe 2002; Tunnacliffe and Lapinski 2003; Feovilova 2003; Lins et al. 2004; Adams et al. 2007; Albertorio et al. 2007; Westh 2008; Hengherr et al. 2008; Zhmakin 2008; Lenné et al. 2009) (TRH, Fig. 1).

Although the detailed mechanism whereby TRH stabilizes bilayer membranes upon dehydration is still a matter of debate, it is clear that this mechanism involves a direct influence of the sugar on the phase properties of the bilayer. Several hypotheses have been proposed [see introduction of Horta et al. (2010a) for an overview], which are not all mutually exclusive (Clegg 2001; Crowe 2002; Horta et al. 2010a).

The phenomenon of anesthesia (Ueda and Kamaya 1984; Rudolph and Antkowiak 2004; Franks 2006) corresponds to a reversible loss of consciousness caused by an anesthetic drug. Other attributes, such as immobility, analgesia, amnesia and muscle relaxation, are closely connected to this phenomenon (Rudolph and Antkowiak 2004; Franks 2008). The exact mechanism of anesthesia is still matter of debate (Fang et al. 1997; Rudolph and Antkowiak 2004; MacCallum and Tieleman 2008; Chau 2010). Depending on the type of CSL (anesthetic), it may involve either an interaction with specific receptors (Rudolph and Antkowiak 2004; Franks 2006, 2008), a direct alteration of the membrane properties (Ueda and Kamaya 1984; Castro et al. 2008), or an indirect influence on membrane-bound proteins (Cantor 1997). In the apparent absence of specific protein receptors for aliphatic alcohol molecules (Foubert et al. 2007), it seems that the mechanism of anesthesia relies in this case on an indirect modulation of the properties of membrane-bound proteins via an alteration of the bilayer phase properties (Chau 2010).

The interaction of alcohols with membranes is further complicated by the biphasic effect (Rowe 1983). Depending on the concentration range, short-chained aliphatic alcohols have an opposite influence on T_m. At low concentrations, T_m decreases with increasing alcohol concentration, whereas at high concentrations, the opposite trend is observed. The concentration at which this reversal takes place for a given alcohol strongly depends on the length of the lipid acyl chains (Rowe 1983). The biphasic effect is explained by the alcohol-induced formation of an interdigitated (ID) phase, where lipid molecules from the two

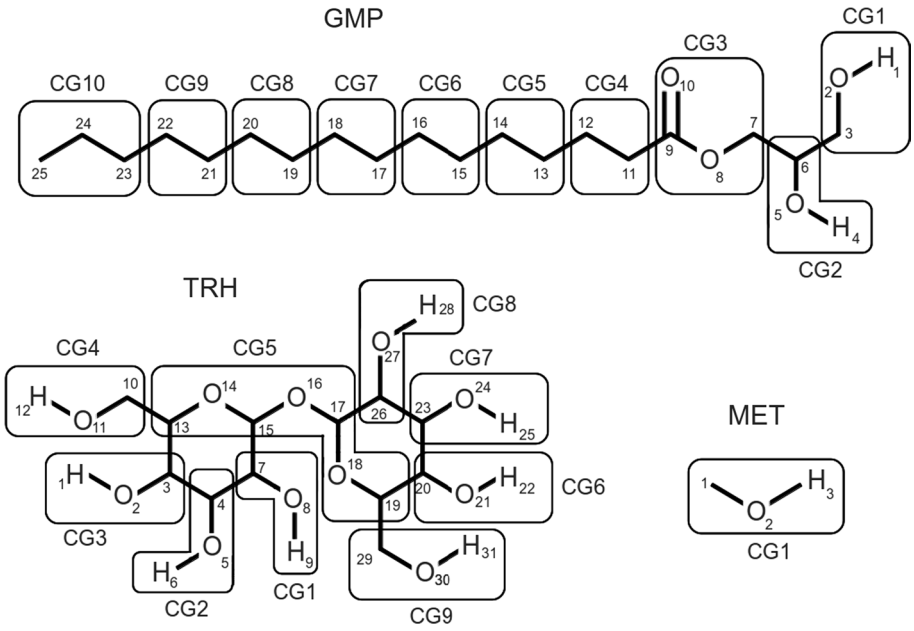

Fig. 1 Chemical structures of the monoglyceride and cosolutes (CSLs) considered in the present study. These are glycerol-1-monopalmitate (GMP), trehalose (TRH), and methanol (MET). The atom numbering refers to the GROMOS molecular topology used in the simulations. The charge group (CG) definitions are also indicated, all CGs being overall neutral. The force-field parameters employed for the three compounds can be found in Tables S.1–S.4 of the Supplementary Material document. The water molecules are represented using the simple point charges (SPC) model (Berendsen et al. 1981)

leaflets of the bilayer interpenetrate (Simon and McIntosh 1984; Chiou et al. 1992). At low alcohol concentrations, the GL phase is destabilized over the LC one, due to the intercalation of alcohol molecules between the lipid headgroups and the resulting increase in the area per lipid, leading to the observed T_m decrease. At high concentrations, the ID phase can be formed, its stability relative to the LC phase increasing with the alcohol concentration, leading to the observed T_m increase. All short-chain aliphatic alcohols, from methanol (MET, Fig. 1) through heptanol, induce interdigitation at sufficiently high concentrations (Ohki et al. 1990; Mou et al. 1994; Holte and Gawrisch 1997). However, longer chain alcohols may induce a different response, presumably because their aliphatic chains are also able to intercalate between the lipid tails (Westermann et al. 1988; Chen et al. 1996; Kranenburg et al. 2004).

Atomistic molecular dynamics (MD) simulations have greatly contributed to the characterization and understanding of the structure, thermodynamics and dynamics of lipid bilayers under various conditions (Marrink et al. 1998; Lindahl and Edholm 2000; Lee et al. 2004, 2005; Skibinski et al. 2005; Chanda and Bandyopadhyay 2006; Patra et al. 2006; Knecht and Marrink 2007; MacCallum and Tieleman 2008; Lyubartsev and Rabinovich 2011; Saito and Shinoda 2011; Yamamoto et al. 2012). These simulations provide information at a spatial (atomic level) and temporal (femtosecond) resolution inaccessible to experiments, concerning system sizes (~10 nm) and timescales (~1 μs) already relevant for the evaluation of thermodynamic properties via statistical mechanics and the comparison with experimental data.

In a series of previous studies by our group, atomistic MD simulations have been used to characterize the effect of alcohols, sugars and other polyhydroxylated CSLs on membranes, in the context of both simple model systems (Geerke et al. 2010; Choutko et al. 2012) and dipalmitoylphosphatidylcholine (DPPC) bilayers (Pereira et al. 2004; Pereira and Hünenberger 2006, 2008a, b; Horta et al. 2010a). However, the biologically most relevant phospholipids such as DPPC remain relatively challenging to simulate, owing to difficulties in the force field design (Anézo et al. 2003; Klauda et al. 2008) and treatment of electrostatic interactions (Tieleman et al. 2002; Anézo et al. 2003; Patra et al. 2003, 2004; Kastenholz and Hünenberger 2004; Cordomí et al. 2007; Reif et al. 2009) (charged or zwitterionic headgroup), and to the slow convergence of system properties with respect to both system size (Takaoka et al. 2000; Anézo et al. 2003; de Vries et al. 2005b; Herce and Garcia 2006; Başтuğ et al. 2006; Klauda et al. 2008; Laner et al. 2013) (long-range correlations) and simulation timescale (Tieleman et al. 1997; Takaoka et al. 2000; de Vries et al. 2005b; Klauda et al. 2006; Nagarajan et al. 2012) (slow conformational relaxation). For this reason, it is also interesting to consider less complex bilayer systems such as monoglyceride lipid systems (Horta et al. 2010b; Horta and Hünenberger 2011; Laner et al. 2013, 2014; Laner and Hünenberger 2014a, b).

A (saturated) monoglyceride is the molecule resulting from the esterification of a single hydroxyl group of glycerol with a (saturated) fatty acid. In addition to being relevant in the context of prebiotic research (Hargreaves et al. 1976; Olasgasti et al. 2014) and technological applications (Krog and Larsson 1968; Morley and Tiddy 1993), these

lipids present a number of key advantages compared to, e.g., DPPC for a computational investigation of the GL↔LC phase transition : (1) the presence of only one aliphatic tail per headgroup, leading to a faster translational, rotational, and conformational relaxation; (2) the limited role of electrostatic interactions (uncharged, non-zwitterionic and moderately polar headgroup), also leading to a faster relaxation and largely avoiding finite-size and approximate-electrostatics artifacts; (3) the absence of a ripple phase (de Vries et al. 2005a) as an intermediate state between the GL and the LC phases; (4) the availability of experimental structural and thermodynamic data (Krog and Larsson 1968; Krog and Borup 1973; Pezron et al. 1990, 1991; Morley and Tiddy 1993; Cassin et al. 1998; Chupin et al. 2001; Sein et al. 2002; van Duynhoven et al. 2005; Alberola et al. 2006). More specifically, glycerol-1-monopalmitate (GMP, Fig. 1) was chosen here as model lipid in view of the availability of a phase diagram for the GMP-water system (Krog and Larsson 1968; Horta et al. 2010b) and of experimental estimates for the area per lipid in the GL and LC phases (Pezron et al. 1990).

In the present study, a GMP bilayer patch is used to investigate the effect of the CSLs TRH and MET on the structural, dynamic and thermodynamic properties of the membrane and on its main transition temperature T_m. To this purpose, 83 MD simulations (each of 600 ns duration) of a GMP bilayer patch of 2 × 8 × 8 lipids are reported and compared, carried out at different temperatures in the range of 302–338 K, either in the absence of CSL [simulations previously reported in Laner et al. (2013)] or in the presence of MET or TRH at three different concentrations.

Methods

Molecular dynamics simulations

All MD simulations were performed using the GROMOS MD++ program (van Gunsteren 2011; Schmid et al. 2012; Kunz et al. 2012), with the 53A6$_{OXY}$ force field (Horta et al. 2011) for the GMP and CSL molecules, along with the simple point charges (SPC) water model (Berendsen et al. 1981). For GMP, this corresponds to force field B in the previous simulations of Laner et al. (2013). The MET model is the 53A6$_{OXY}$ model (Horta et al. 2011) [and not the rigid model of Walser et al. (2000)], and the TRH model is based on that of Lins and Hünenberger (2005), with appropriate adjustments of the charges and Lennard-Jones interaction parameters to 53A6$_{OXY}$. The relevant force-field parameters are summarized in Fig. 1 and Tables S.1–S.4 of the Supplementary Material document.

The simulations were carried out under periodic boundary conditions based on rectangular boxes containing a hydrated GMP bilayer patch of 2 × 8 × 8 lipid molecules in the *xy*-plane, leading to a total number of 128 lipid molecules in the systems. Both leaflets consisted of a racemic mixture of the *R* and *S* enantiomers of the GMP molecule. A variable number of CSL molecules was possibly added: (1) none [simulations labeled P_N, i.e., pure lipid in water; previously reported in Laner et al. (2013) under the label B_L]; (2) 53 molecules of TRH (simulations labeled T_N); or (3) either 120, 240 or 480 molecules of MET (simulations labeled M_L, M_M and M_E, respectively, i.e., low, medium or elevated MET content).

For both the pure-lipid simulations (P_N) and the simulations in the presence of TRH (T_N), three hydration levels were considered, which are distinguished by the letters F (full), H (half), or Q (quarter), respectively. The full hydration regime was defined based on the phase diagram of the GMP-water system (Krog and Larsson 1968; Horta et al. 2010b), where the main transition temperature T_m is seen to become independent of the hydration level above 36 % w/w water content, which corresponds to about 6.7 water molecules per lipid. Accordingly, the numbers of water molecules in the simulated systems were set to 853 (F), 427 (H) and 213 (Q). The simulations in the presence of MET (M_L, M_M and M_E) were all carried out at full hydration, i.e., with 853 water molecules.

Newton's equations of motion were integrated using the leap-frog scheme (Hockney 1970) with a timestep of 2 fs. All solute bond lengths (GMP and CSLs) were constrained by application of the SHAKE algorithm (Ryckaert et al. 1977) with a relative geometric tolerance of 10^{-4}. The full rigidity of the water molecules was enforced by application of the SETTLE algorithm (Miyamoto and Kollman 1992). The center of mass translational motion of the computational box was removed every 0.2 ps.

The simulations were carried out in the isothermal-isobaric ensemble with a reference pressure P of 1 bar and reference temperatures T ranging from 302 to 338 K. The temperature was maintained by weakly coupling (Berendsen et al. 1984) the solute+CSL and solvent degrees of freedom separately to temperature baths at temperature T, using a relaxation time of 0.1 ps. The pressure was maintained by weakly coupling (Berendsen et al. 1984) the particle coordinates and box dimensions in the *xy*-plane and along the *z*-axis separately [semi-anisotropic pressure scaling (Klauda et al. 2008); systems P_N and T_N], or along all three axes separately (fully anisotropic pressure scaling; systems M_L, M_M and M_E) to pressure baths at pressure P, using a relaxation time of 1 ps and an isothermal compressibility of 4.575×10^{-4} (kJ mol^{-1} nm^{-3})$^{-1}$ as appropriate for biomolecular systems (van Gunsteren et al. 1996).

The non-bonded interactions were calculated using a twin-range scheme (van Gunsteren et al. 1990, 1996), with short-range and long-range cutoff distances set to

0.8 and 1.4 nm, respectively, and an update frequency of five timesteps for the short-range pairlist and intermediate-range interactions. A reaction-field correction (Barker and Watts 1973; Tironi et al. 1995) was applied to account for the mean effect of electrostatic interactions beyond the long-range cutoff distance, using a relative dielectric permittivity of 61 as appropriate for the SPC water model (Heinz et al. 2001). All simulations were carried out for a duration of 600 ns after equilibration and configurations were saved to file every 10 ps for subsequent analysis.

Simulated systems

A total number of 83 simulations were carried out, differing by: (1) the possible presence and type of the CSL (P vs. T vs. M); (2) the number of CSL molecules in the system (N vs. L vs. M vs. E); (3) the hydration level (F vs. H vs. Q); (4) the initial configuration (GL vs. LC); (5) the temperature T (from 302, 306 or 318 K, depending on the system, to 338 K in steps of 4 K).

Only a subset of the possible combinations was considered, the corresponding systems and conditions being summarized in Table 1. In particular, the combinations involving MET (M_L, M_M or M_E) with a water content below full hydration (H or Q) were omitted, since initial simulations with a high MET content (M_E) at lower hydration led to the partial or complete dissolution of the bilayer (results not shown), as expected experimentally (Ly and Longo 2004) and already observed in previous simulations involving ethanol (Gurtovenko and Anwar 2009). The lowest temperature considered was initially set to 318 K. However, in the presence of MET, this was not sufficient to observe a stable GL phase. The minimal temperature was thus decreased to 306 K for system M_E or 302 K for systems M_L and M_M. All simulations initiated from a GL structure were carried out at up to ten different temperatures in steps of 4 K, as an attempt to bracket T_m within ± 2 K. However, the simulations initiated from a LC structure were only performed at the two extreme temperatures. In this article, each of the 83 simulations (Table 1) is uniquely identified by a string consisting in sequence of the letters P, T or M (system), N, L, M or E (CSL content; subscript), F, H or Q (hydration level), and GL or LC (initial configuration; subscript), followed by the temperature T.

Table 1 Simulated systems and simulation conditions

Simulation	CSL	n_C	c_C [% w/w]	Hydration	n_W	c_W [% w/w]	Starting configuration	T [K]
$P_NF_{GL}\mathcal{T}$	None	0	–	F	853	36.3	GL	$\mathcal{T} \in \{318–338\}$
$P_NF_{LC}\mathcal{T}$	None	0	–	F	853	36.3	LC	$\mathcal{T} \in \{318, 338\}$
$P_NH_{GL}\mathcal{T}$	None	0	–	H	427	18.2	GL	$\mathcal{T} \in \{318–338\}$
$P_NH_{LC}\mathcal{T}$	None	0	–	H	427	18.2	LC	$\mathcal{T} \in \{318, 338\}$
$P_NQ_{GL}\mathcal{T}$	None	0	–	Q	213	9.1	GL	$\mathcal{T} \in \{318–338\}$
$P_NQ_{LC}\mathcal{T}$	None	0	–	Q	213	9.1	LC	$\mathcal{T} \in \{318, 338\}$
$T_NF_{GL}\mathcal{T}$	TRH	53	42.9	F	853	36.3	GL	$\mathcal{T} \in \{318–338\}$
$T_NF_{LC}\mathcal{T}$	TRH	53	42.9	F	853	36.3	LC	$\mathcal{T} \in \{318, 338\}$
$T_NH_{GL}\mathcal{T}$	TRH	53	42.9	H	427	18.2	GL	$\mathcal{T} \in \{318–338\}$
$T_NH_{LC}\mathcal{T}$	TRH	53	42.9	H	427	18.2	LC	$\mathcal{T} \in \{318, 338\}$
$T_NQ_{GL}\mathcal{T}$	TRH	53	42.9	Q	213	9.1	GL	$\mathcal{T} \in \{318–338\}$
$T_NQ_{LC}\mathcal{T}$	TRH	53	42.9	Q	213	9.1	LC	$\mathcal{T} \in \{318, 338\}$
$M_LF_{GL}\mathcal{T}$	MET	120	9.1	F	853	36.3	GL	$\mathcal{T} \in \{302–338\}$
$M_LF_{LC}\mathcal{T}$	MET	120	9.1	F	853	36.3	LC	$\mathcal{T} \in \{302, 338\}$
$M_MF_{GL}\mathcal{T}$	MET	240	18.2	F	853	36.3	GL	$\mathcal{T} \in \{302–338\}$
$M_MF_{LC}\mathcal{T}$	MET	240	18.2	F	853	36.3	LC	$\mathcal{T} \in \{302, 338\}$
$M_EF_{GL}\mathcal{T}$	MET	480	36.4	F	853	36.3	GL	$\mathcal{T} \in \{306–338\}$
$M_EF_{LC}\mathcal{T}$	MET	480	36.4	F	853	36.3	LC	$\mathcal{T} \in \{306, 338\}$

For each simulation, the different columns report the simulation label, the cosolute (CSL) type (none, TRH for trehalose, or MET for methanol), the number n_C of CSL molecules, the CSL concentration c_C (by weight relative to the lipids), the hydration level relative to full hydration (F, H or Q for full, half, or quarter), the number n_W of water molecules, the water concentration c_W (by weight relative to the lipids), the starting configuration (GL for gel or LC for liquid crystal) and the reference temperature T. In all cases, the simulations involved a glycerol-1-monopalmitate (GMP) bilayer patch of $2 \times 8 \times 8$ lipids (number n_L of lipids equal to 128) and were carried out for 600 ns at the reference pressure $P = 1$ bar. For compactness, a single entry is provided for each set of simulations carried out at different temperatures T (value in Kelvin noted generically $\mathcal{T}$ in the simulation label). For example, the notation $\mathcal{T} \in \{318–338\}$ indicates a set of six simulations at temperatures T ranging from 318 to 338 K in steps of 4 K, and the notation $\mathcal{T} \in \{318, 338\}$ indicates a set of two simulations carried out at temperatures T of 318 and 338 K

The initial configurations for the system without CSL were generated as described in Laner et al. (2013). The production simulations for the set P_N, already reported in Laner et al. (2013), were initiated directly from these six configurations and carried out at the indicated temperatures. For the simulations including a CSL, all water molecules were removed, and the CSL molecules were inserted by random placement. The system was solvated with the appropriate number of water molecules. It was then heated to 600 K with position constraints on the lipid atoms, in order to allow for faster relaxation of the CSL and water molecules, followed by a thermalization step of 1.2 ns to equilibrate the system at a temperature ensuring the stability of either the GL (302, 306 or 318 K, depending on the system) or the LC (338 K) phase, carried out in the presence of progressively decreasing position restraints on the lipid atoms. Each run was continued without restraints during 120 ns at the same temperature for further equilibration, resulting in 12 initial configurations (GL or LC for T_NF, T_NH, T_NQ, M_LF, M_MF and M_EF). All production simulations were initiated directly from these configurations and carried out at the indicated simulation temperatures.

Trajectory analysis

The simulations were analyzed in terms of the following properties: (1) area per lipid a_{xy}; (2) carbon-hydrogen order parameters S_{CH} (C_n) of the 14 methylene groups (C_n, with $n = 2$–15; atoms numbered 11–24 in Fig. 1) and corresponding chain-averaged value S_{chn}; (3) bilayer thickness d_z; (4) volume per lipid v_{xyd}; (5) average numbers N of intermolecular hydrogen bonds (H-bonds) between the different species; (6) lipid lateral diffusion coefficients D_{xy}; (7) lipid rotational (R) or wobbling (W) relaxation times τ and residual correlations c (τ_1^R, c_1^R, τ_2^R, c_2^R, τ_1^W, c_1^W, τ_2^W, c_2^W; distinguishing fast and slow decays by the indexes 1 and 2); (8) distribution profiles $P(z)$ of different atoms along the bilayer normal; (9) single-lipid and collective tilt angles θ and Θ, respectively, of the acyl chains relative to the bilayer normal; (10) phase-assignment descriptor η.

The procedures employed for the first seven types of analyses have been described previously (Laner et al. 2013) and will not be repeated here. Three of these parameters (a_{xy}, S_{chn}, d_z) were monitored as a function of time, as indicators of a phase transition (for S_{chn} and d_z, based on successive 1.2 ns time windows). Averages of all of these parameters were calculated over the last 24 ns of the simulations, as structural and dynamic characteristics of the final phase. Only the H-bond analysis differs slightly from Laner et al. (2013), due to the possible presence of CSL molecules in the system.

Here, the occurring intermolecular H-bonds were classified according to the different pairs of species present in the simulations, namely intra-layer lipid-lipid N_{LL}^{intra}, inter-layer lipid-lipid N_{LL}^{inter}, lipid-CSL N_{LC}, lipid-water N_{LW}, CSL-CSL N_{CC}, CSL-water N_{CW} and water-water N_{WW}. Inter-layer H-bonds, as opposed to intra-layer ones, refer to H-bonds possibly occurring between the opposite leaflets of two periodic copies of the bilayer. The corresponding average occurrences are reported on a per-molecule basis, namely as: $2n_L^{-1}N_{LL}^{intra}$, $2n_L^{-1}N_{LL}^{inter}$, $n_L^{-1}N_{LC}$ and $n_L^{-1}N_{LW}$ for the lipids; $n_C^{-1}N_{LC}$, $2n_C^{-1}N_{CC}$ and $n_C^{-1}N_{CW}$ for the CSL; $n_W^{-1}N_{LW}$, $n_W^{-1}N_{CW}$ and $2n_W^{-1}N_{WW}$ for water. Here, n_L, n_C and n_W are the total numbers of lipid, CSL and water molecules, respectively, in the simulated systems (Table 1). The corresponding total numbers of H-bonds per lipid, per CSL or per water molecule are also reported as N_L^{tot}, N_C^{tot} and N_W^{tot}, respectively. Patterns of H-bonded bridging (Pereira et al. 2004; Pereira and Hünenberger 2006, 2008a, b; Horta et al. 2010a) were also monitored, i.e., the number of water molecules n_W^m and CSL molecules n_C^m being simultaneously H-bonded to a given number m of lipid molecules (as acceptor or as donor, and possibly via more than one H-bond). Note that the values of n_W^m and n_C^m add up to n_W and n_C, respectively.

The procedures employed for the last three types of analyses are the following. The distribution profiles $P(z)$ were calculated as normalized probability distributions along the bilayer normal (z-axis) for specific atoms, namely the headgroup oxygen atoms (atoms 2 and 5 in Fig. 1), the ester oxygen atoms (atoms 8 and 10), the terminal methyl group (atom 25), the CSL oxygen atoms (all oxygen atoms) and the water oxygen atoms. For the lipid atoms, the calculation distinguished between lipids of the bottom and top leaflets. Averaging was performed over the last 24 ns of the simulations.

The tilt angle θ_n of a given lipid n in a given trajectory configuration is defined as the angle between the bilayer normal and the head-tail vector of the lipid, connecting the carbonyl carbon atom (atom 9 in Fig. 1) and the terminal methyl group (atom 25) of the chain, choosing the normal direction in such a way that $\theta_n \leq 90°$. The single-lipid tilt angle θ is obtained by averaging the value of θ_n over the individual lipids n in a given trajectory configuration. The collective tilt angle Θ is defined as the angle between the bilayer normal and the vector sum of the head-tail vectors of all lipids in a given trajectory configuration, respecting the same convention for the normal direction. The values of θ and Θ were averaged over the last 24 ns of the simulations.

Finally, the idea of the phase-assignment descriptor is to tentatively ascribe a phase to each trajectory configuration. This was done by means of a single-configuration descriptor η defined as

$$\eta = \begin{cases} \text{LC} & \text{if } a \geq a_c\,, h \leq h_c \text{ and } g > g_c \\ \text{GL} & \text{if } a < a_c\,, h > h_c \text{ and } g > g_c \\ \text{ID} & \text{if } a \geq a'_c\,, h \leq h'_c \text{ and } g \leq g_c \\ \text{UN} & \text{otherwise} \end{cases}, \quad (1)$$

where the different phases are liquid crystal (LC), gel (GL), interdigitated (ID), and unassigned (UN). Here, a is the area per lipid (a_{xy}, see above), h the headgroup-headgroup distance across the bilayer, and g the tail-tail distance across the bilayer. The parameters h and g are calculated for a trajectory configuration by periodic gathering of the lipid atoms along the z-direction with the bilayer midplane (average of the z-coordinates of the 128 terminal methyl groups) at $z = 0$, and measurement of the average z-distance between the 64 glycerol central carbon (atom 6 in Fig. 1) atoms (h) or the 64 tail methyl (atom 25) united atoms (g) of the bottom and top layers, respectively (top minus bottom). The cutoff values in Eq. 1 were defined by visual inspection of the sampled phases and correlation with their a, h and g values. They were set to $a_c = 0.29$ nm^2, $a'_c = 0.35$ nm^2, $h_c = 3.9$ nm, $h'_c = 2.9$ nm and $g_c = -0.5$ nm for all systems.

Results and discussion

Equilibrium properties

To characterize the influence of the CSL, CSL content and hydration level on the structural and dynamic properties of the bilayer in its two main phases (GL or LC), equilibrium simulations are discussed first. For simplicity, this is done here by considering the simulations initiated from a GL structure and carried out at the lowest temperature (302 K for M_L and M_M, 306 K for M_E, and 318 K for P_N and T_N), and the simulations initiated from a LC structure and carried out at the highest temperature (338 K). For these two sets of simulations, the starting configuration is the one that is thermodynamically stable at the given temperature so that no phase transitions are observed. The average values of key properties calculated over the last 24 ns of these 18 simulations are reported in Table 2 (structural properties and phase assignment), Tables 3 and 4 (H-bonding properties; see also Fig. 2 for a summary scheme), Fig. 3 (distribution profiles), and Table 5 (dynamic properties). The

Table 2 Average structural properties calculated from a subset of simulations corresponding to equilibrium conditions

Simulation	Final phase	a_{xy} [nm^2]	S_{chn}	d_z [nm]	v_{xyd} [nm^3]	θ [deg]	Θ [deg]	GL [%]	LC [%]	ID [%]	UN [%]	h [nm]	g [nm]
$P_NF_{GL}318$	GL	0.243	0.305	4.00	0.456	20.5	15.0	100.0	0.0	0.0	0.0	4.14	0.42
$P_NF_{LC}338$	LC	0.328	0.152	3.09	0.483	32.4	7.0	0.0	100.0	0.0	0.0	3.31	0.36
$P_NH_{GL}318$	GL	0.241	0.282	3.91	0.449	25.3	24.3	100.0	0.0	0.0	0.0	4.12	0.39
$P_NH_{LC}338$	LC	0.337	0.147	3.03	0.485	34.1	7.0	0.0	100.0	0.0	0.0	3.24	0.36
$P_NQ_{GL}318$	GL	0.242	0.291	3.98	0.456	25.0	24.1	100.0	0.0	0.0	0.0	4.12	0.38
$P_NQ_{LC}338$	LC	0.340	0.143	2.99	0.484	34.9	6.7	0.0	100.0	0.0	0.0	3.19	0.35
$T_NF_{GL}318$	GL	0.239	0.297	3.94	0.448	22.3	19.8	100.0	0.0	0.0	0.0	4.19	0.42
$T_NF_{LC}338$	LC	0.343	0.128	2.96	0.482	35.1	7.2	0.0	100.0	0.0	0.0	3.17	0.34
$T_NH_{GL}318$	GL	0.238	0.296	3.98	0.453	23.0	20.7	100.0	0.0	0.0	0.0	4.14	0.37
$T_NH_{LC}338$	LC	0.348	0.130	2.84	0.467	36.5	7.9	0.0	100.0	0.0	0.0	3.10	0.35
$T_NQ_{GL}318$	GL	0.235	0.322	4.01	0.448	21.2	19.2	100.0	0.0	0.0	0.0	4.22	0.42
$T_NQ_{LC}338$	LC	0.372	0.117	2.68	0.477	38.7	8.4	0.0	100.0	0.0	0.0	2.94	0.28
$M_LF_{GL}302$	GL	0.233	0.331	4.05	0.450	22.5	20.9	100.0	0.0	0.0	0.0	4.22	0.38
$M_LF_{LC}338$	LC	0.368	0.132	2.83	0.498	37.5	6.8	0.0	100.0	0.0	0.0	3.03	0.30
$M_MF_{GL}302$	GL	0.242	0.306	4.03	0.464	20.9	14.8	100.0	0.0	0.0	0.0	4.09	0.33
$M_MF_{LC}338$	LC	0.399	0.124	2.60	0.494	39.6	7.6	0.0	100.0	0.0	0.0	2.86	0.24
$M_EF_{GL}306$	GL	0.238	0.301	4.08	0.463	23.3	16.7	100.0	0.0	0.0	0.0	4.09	0.40
$M_EF_{LC}338$	LC	0.452	0.076	2.41	0.518	43.4	8.3	0.0	100.0	0.0	0.0	2.63	0.19
$M_MF_{LC}302$	ID	0.366	0.411	2.32	0.405	10.5	4.1	0.0	6.0	94.0	0.0	2.77	−1.19

This subset encompasses the simulations started from a structure appropriate for the GL phase at reference temperatures $T = 302$ (systems M_L and M_M), 306 (system M_E) or 318 K (all other systems), as well as from a structure appropriate for the LC phase at reference temperature $T = 338$ K, for the different CSLs (P, T or M), numbers of CSL molecules (N, L, M or E) and hydration levels (F, H or Q). As an example for the ID phase, values for the simulation $M_MF_{LC}302$ are also provided (last line). The quantities reported are the area per lipid a_{xy}, the chain-averaged order parameter S_{chn}, the bilayer thickness d_z, the volume per lipid v_{xyd}, the single-lipid tilt angle θ and the collective tilt angle Θ, averaged over the last 24 ns of the simulations and appropriate for the indicated final phase. The percentages of the configurations assigned to the different phases (GL, LC, ID or UN) over the entire 600 ns simulation time are also reported, along with the phase-assignment parameters h and g used in Eq. 1, averaged over the last 24 ns. The simulation labels and conditions are summarized in Table 1. Corresponding data for the entire set of 83 simulations can be found in Tables S.5–S.7 of the Supplementary Material document

Table 3 Average hydrogen-bonding (H-bonding) properties calculated from a subset of simulations corresponding to equilibrium conditions

Simulation	$\frac{2N_{LL}^{inter}}{n_L}$	$\frac{2N_{LL}^{intra}}{n_L}$	$\frac{N_{LW}}{n_L}$	$\frac{N_{LW}}{n_W}$	$\frac{N_{LC}}{n_L}$	$\frac{N_{LC}}{n_C}$	$\frac{N_{CW}}{n_C}$	$\frac{N_{CW}}{n_W}$	$\frac{2N_{CC}}{n_C}$	$\frac{2N_{WW}}{n_W}$	N_L^{tot}	N_C^{tot}	N_W^{tot}
$P_NF_{GL}318$	0.00	1.96	2.22	0.33	–	–	–	–	–	2.96	4.2	–	3.3
$P_NF_{LC}338$	0.01	1.43	2.82	0.42	–	–	–	–	–	2.73	4.3	–	3.2
$P_NH_{GL}318$	0.03	2.06	2.06	0.62	–	–	–	–	–	2.66	4.1	–	3.3
$P_NH_{LC}338$	0.19	1.39	2.65	0.80	–	–	–	–	–	2.29	4.2	–	3.1
$P_NQ_{GL}318$	0.21	2.08	1.82	1.09	–	–	–	–	–	2.13	4.1	–	3.2
$P_NQ_{LC}338$	0.49	1.48	2.17	1.30	–	–	–	–	–	1.67	4.1	–	3.0
$T_NF_{GL}318$	0.00	2.06	1.68	0.25	0.32	0.78	10.13	0.63	3.53	2.36	4.1	14.4	3.2
$T_NF_{LC}338$	0.00	1.45	2.22	0.33	0.49	1.18	9.26	0.57	3.20	2.19	4.2	13.6	3.1
$T_NH_{GL}318$	0.00	2.11	1.42	0.42	0.48	1.16	7.77	0.96	5.16	1.79	4.0	14.1	3.2
$T_NH_{LC}338$	0.00	1.50	1.80	0.54	0.79	1.91	6.98	0.87	4.24	1.62	4.1	13.1	3.0
$T_NQ_{GL}318$	0.00	2.19	0.97	0.58	0.77	1.86	5.54	1.38	6.40	1.15	3.9	13.8	3.1
$T_NQ_{LC}338$	0.02	1.50	1.32	0.79	1.20	2.90	4.35	1.08	5.35	1.06	4.0	12.6	2.9
$M_LF_{GL}302$	0.00	2.17	1.75	0.26	0.24	0.25	1.91	0.27	0.22	2.81	4.2	2.4	3.3
$M_LF_{LC}338$	0.01	1.24	2.58	0.39	0.40	0.43	1.56	0.22	0.19	2.50	4.2	2.2	3.1
$M_MF_{GL}302$	0.00	2.01	1.71	0.26	0.47	0.25	1.68	0.47	0.40	2.57	4.2	2.3	3.3
$M_MF_{LC}338$	0.01	1.11	2.36	0.35	0.71	0.38	1.43	0.40	0.34	2.31	4.2	2.2	3.1
$M_EF_{GL}306$	0.01	2.07	1.39	0.21	0.62	0.17	1.44	0.81	0.66	2.19	4.1	2.3	3.2
$M_EF_{LC}338$	0.01	0.92	2.06	0.31	1.15	0.31	1.24	0.70	0.57	2.00	4.1	2.1	3.0
$M_MF_{LC}302$	0.00	1.54	2.22	0.33	0.58	0.31	1.62	0.46	0.38	2.49	4.3	2.3	3.3

This subset encompasses the simulations started from a structure appropriate for the GL phase at reference temperature $T = 302$ (systems M_L and M_M), 306 (system M_E) or 318 K (all other systems), as well as from a structure appropriate for the LC phase at reference temperature $T = 338$ K, for the different CSLs (P, T or M), numbers of CSL molecules (N, L, M or E) and hydration levels (F, H or Q). As an example for the ID phase, values for the simulation $M_MF_{LC}302$ are also provided (last line). The quantities reported are the number of inter-layer ($2n_L^{-1}N_{LL}^{inter}$) and intra-layer ($2n_L^{-1}N_{LL}^{intra}$) lipid-lipid H-bonds per lipid, the number of lipid-water H-bonds per lipid ($n_L^{-1}N_{LW}$), or per water ($n_W^{-1}N_{LW}$), the number of lipid-CSL H-bonds per lipid ($n_L^{-1}N_{LC}$), or per CSL ($n_C^{-1}N_{LC}$), the number of CSL-water H-bonds per CSL ($n_C^{-1}N_{CW}$), or per water ($n_W^{-1}N_{CW}$), the number of CSL-CSL H-bonds per CSL ($2n_C^{-1}N_{CC}$), and the number of water-water H-bonds per water ($2n_W^{-1}N_{WW}$). The total numbers of H-bonds per lipid (N_L^{tot}), per CSL (N_C^{tot}) and per water (N_W^{tot}) are also reported. The data is averaged over the last 24 ns of the simulations. The simulation labels and conditions are summarized in Table 1. Corresponding data for the entire set of 83 simulations can be found in Tables S.8–S.10 of the Supplementary Material document

simulations in the absence of CSL (P_N) are the same as those reported in Laner et al. (2013), and are discussed in more details therein.

Concerning the structural properties (Table 2), the main observations in the absence of CSL (system P_N) are that (Laner et al. 2013): (1) the area per lipid a_{xy} is systematically lower for the GL compared to the LC phase; (2) the values are essentially independent of the hydration level for the GL phase and increase slightly upon decreasing the hydration level for the LC phase; (3) the values at full hydration, 0.243 (GL) and 0.328 (LC) nm^2, agree well with the corresponding experimental estimates of 0.22 and 0.31 nm^2, respectively (Pezron et al. 1990); (4) the trends observed in terms of the chain-averaged order parameter S_{chn} and the bilayer thickness d_z are anti-correlated with those observed in terms of a_{xy}; (5) the relative changes in the volume per lipid v_{xyd} are of small relative magnitudes compared to those in a_{xy} and d_z.

In the presence of CSLs, the area per lipid a_{xy} is still systematically lower for the GL compared to the LC phase. Whereas the area per lipid in the GL phase is essentially insensitive to the presence of a CSL, as it was to the hydration level in the pure-bilayer systems, the CSLs induce a lateral expansion in the LC phase, slight and nearly concentration-independent for TRH (except maybe at the lowest hydration), and more pronounced and concentration-dependent for MET.

As was the case when varying the hydration level in the absence of CSL, the trends in the chain-averaged order parameter S_{chn} and in the bilayer thickness d_z are anti-correlated with those in a_{xy}. In particular, in the presence of a CSL, both parameters are still systematically higher for the GL compared to the LC phase. For the GL phase, the two parameters are essentially insensitive to the presence of a CSL. For the LC phase, both CSLs induce an increase in the extent of disorder and a decrease in the thickness of the bilayer, slight and nearly concentration-independent for TRH (except maybe at the lowest hydration), more pronounced and concentration-dependent for MET.

Table 4 Extent of hydrogen-bonded (H-bonded) bridging of the lipids calculated from a subset of simulations corresponding to equilibrium conditions

Simulation	$n_L^{-1}(n_W - n_W^o)$	$(n_W - n_W^o)^{-1} n_W^m$				$n_L^{-1}(n_C - n_C^o)$	$(n_C - n_C^o)^{-1} n_C^m$							
		$m = 1$	2	3	4		$m = 1$	2	3	4	5	6	7	8
$P_NF_{GL}318$	1.68	0.73	0.22	0.05	0.00	–	–	–	–	–	–	–	–	–
$P_NF_{LC}338$	2.22	0.76	0.20	0.03	0.00	–	–	–	–	–	–	–	–	–
$P_NH_{GL}318$	1.54	0.72	0.23	0.05	0.00	–	–	–	–	–	–	–	–	–
$P_NH_{LC}338$	1.95	0.69	0.25	0.05	0.00	–	–	–	–	–	–	–	–	–
$P_NQ_{GL}318$	1.21	0.61	0.30	0.09	0.01	–	–	–	–	–	–	–	–	–
$P_NQ_{LC}338$	1.41	0.57	0.32	0.10	0.01	–	–	–	–	–	–	–	–	–
$T_NF_{GL}318$	1.21	0.68	0.25	0.06	0.00	0.15	0.40	0.29	0.18	0.09	0.04	0.01	0.01	0.00
$T_NF_{LC}338$	1.70	0.74	0.22	0.04	0.00	0.23	0.42	0.28	0.16	0.08	0.04	0.01	0.00	0.00
$T_NH_{GL}318$	1.00	0.66	0.27	0.07	0.00	0.21	0.36	0.29	0.20	0.10	0.04	0.01	0.00	0.00
$T_NH_{LC}338$	1.35	0.72	0.23	0.04	0.00	0.33	0.32	0.29	0.20	0.11	0.05	0.02	0.01	0.00
$T_NQ_{GL}318$	0.66	0.62	0.29	0.08	0.01	0.30	0.31	0.25	0.19	0.12	0.07	0.03	0.02	0.00
$T_NQ_{LC}338$	0.96	0.69	0.26	0.05	0.00	0.39	0.16	0.24	0.24	0.18	0.10	0.05	0.02	0.01
$M_LF_{GL}302$	1.29	0.71	0.23	0.05	0.00	0.19	0.77	0.22	0.01	0.00	–	–	–	–
$M_LF_{LC}338$	2.07	0.78	0.19	0.03	0.00	0.34	0.81	0.18	0.00	–	–	–	–	–
$M_MF_{GL}302$	1.26	0.70	0.24	0.06	0.00	0.38	0.77	0.22	0.01	–	–	–	–	–
$M_MF_{LC}338$	1.93	0.80	0.18	0.02	0.00	0.61	0.83	0.16	0.00	–	–	–	–	–
$M_EF_{GL}306$	1.00	0.68	0.26	0.06	0.00	0.51	0.78	0.21	0.01	0.00	–	–	–	–
$M_EF_{LC}338$	1.72	0.82	0.16	0.02	0.00	1.01	0.87	0.13	0.00	0.00	–	–	–	–
$M_MF_{LC}302$	1.71	0.74	0.22	0.04	0.00	0.49	0.82	0.18	0.00	0.00	–	–	–	–

This subset encompasses the simulations started from a structure appropriate for the GL phase at reference temperature $T = 302$ (systems M_L and M_M), 306 (system M_E) or 318 K (all other systems), as well as from a structure appropriate for the LC phase at reference temperature $T = 338$ K, for the different CSLs (P, T or M), numbers of CSL molecules (N, L, M or E) and hydration levels (F, H or Q). As an example for the ID phase, the values for simulation $M_MF_{LC}302$ are also provided (last line). The quantities n_W^m and n_C^m with $m = 0$–8 represent the numbers of water and CSL molecules, respectively, being simultaneously H-bonded (as acceptor or as donor, and possibly via more than one H-bond) to a given number m of lipid molecules. These numbers add up to the total number of water molecules n_W and CSL molecules n_C in the simulated system (Table 1). The quantities reported are the average numbers of lipid-bound water molecules $n_L^{-1}(n_W - n_W^o)$ and CSL molecules $n_L^{-1}(n_C - n_C^o)$ on a per-lipid basis, along with the fractions of these bound molecules $(n_W - n_W^o)^{-1} n_W^m$ and $(n_C - n_C^o)^{-1} n_C^m$ being simultaneously H-bonded to a given number m of lipid molecules. The notation 0.00 refers to a value below 0.005, while absent entries correspond to a value of exactly zero. The data is averaged over the last 24 ns of the simulations. The simulation labels and conditions are summarized in Table 1

The volume per lipid v_{xyd} evidences relative changes of small magnitudes compared to those in a_{xy} and d_z, due to a compensation in the variations of these two anti-correlated parameters within their product. This average volume is only slightly lower for the GL compared to the LC phase, i.e., the disorder increase accompanying a GL→LC transition causes a relatively limited decrease in the effective packing density of the lipid atoms within the bilayer, but a much more pronounced change in the packing anisotropy (stretching and thinning of the membrane). For the GL phase, v_{xyd} is remarkably invariant across all systems, with values in the range of 0.448–0.464 nm^3. For the LC phase, the value in the absence of CSL is about 0.485 nm^3, irrespective of the hydration level. Interestingly, TRH at high concentration decreases the volume per lipid whereas MET at high concentration increases this volume. The value of 0.485 nm^3 for this phase corresponds to about 0.030 nm^3 per methylene group, assuming an equivalent volume of 16 methylene groups per chain. This value is identical to the corresponding group increment for liquid alkanes at room temperature and ambient pressure (Small 1984). In contrast, the value of about 0.455 nm^3 for the GL phase leads to 0.028 nm^3 per methylene group, noticeably larger than the estimate of 0.025 nm^3 for solid alkanes (Small 1984). For comparison, corresponding experimentally inferred estimates for DPPC are 0.027 and 0.024 nm^3 for the GL phase (Nagle and Wiener 1988; Koenig and Gawrisch 2005) at 0 and 20 °C, respectively, and 0.027 nm^3 for the LC phase (Nagle and Wiener 1988; Armen et al. 1998) at 50 °C. However, these estimates are indirect and affected by important uncertainties, certainly larger than those affecting the experimental densities of pure alkanes in the solid and liquid phases.

The analysis of the single-lipid and collective tilt angles θ and Θ, respectively, underlines the profound structural difference between the GL and LC phases. For the GL

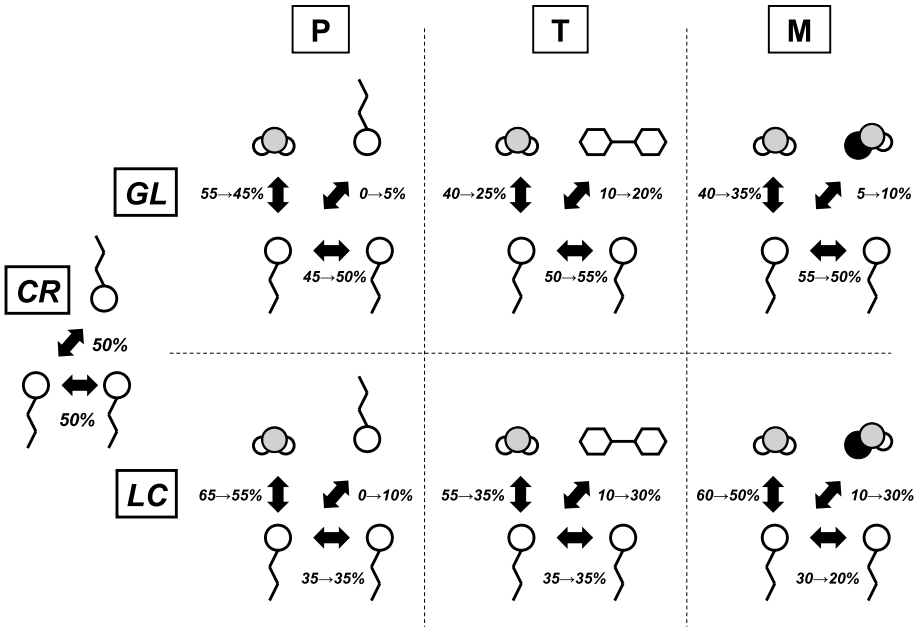

Fig. 2 Schematic illustration of the lipid-environment H-bond distributions for a GMP bilayer in different phases and environments. The total number of lipid-environment H-bonds per lipid is about four in all cases (N_L^{tot} in Table 3; range 3.9–4.3). This number is partitioned into intra-layer lipid-lipid, inter-layer lipid-lipid, lipid-water and lipid-CSL contributions (based on the entries $2n_L^{-1}N_{LL}^{inter}$, $2n_L^{-1}N_{LL}^{intra}$, $n_L^{-1}N_{LW}$ and $n_L^{-1}N_{LC}$ of Table 3), expressed in percent and rounded to the closest multiple of five. The environments considered are: pure monoglyceride crystal [CR; H-bond distribution based on Larsson (1966), Goto and Takiguchi (1985), Goto et al. (1988)]; pure hydrated bilayer (P); hydrated bilayer in the presence of TRH (T); hydrated bilayer in the presence of MET (M). For the three latter environments, the GL and LC phases are distinguished and the *arrows* indicate a decrease in the hydration at constant CSL content (P, T) or an increase in the CSL content at constant hydration (M), i.e., the numbers to the *left* of the *arrows* correspond to simulations P_NF, T_NF and M_LF, and those to the *right* of the *arrows* to simulations P_NQ, T_NQ and M_EF.

phase, θ and Θ are on the order of 20°–25° and 15°–25°, respectively. This indicates that the tilting of the chains is almost exclusively of a collective nature. For comparison, an experimentally inferred estimate for DPPC in the GL phase (Katsaras et al. 1992) is 21.5°, with similar values being reported in simulations (Bennet et al. 2009; Chen et al. 2011). For the LC phase, θ and Θ are on the order of 35°–45° and 7°–8°, respectively. Interestingly, θ is actually higher than in the GL phase, i.e., individually, the chains are on average more pronouncedly tilted. Note that in the context of chains that present a non-negligible fraction of *gauche* conformations, the occurrence of kinks may also contribute to an apparent tilting of the head-tail vector (Douliez et al. 1998), i.e., to θ. However, the tilt (kink) directions of the individual lipids are orientationally randomized, resulting in a collective tilt angle Θ that is much lower compared to the GL phase. Still, it is interesting to observe the existence of a residual collective tilt of about 7°–8° , even in the LC phase.

The reduction of the hydration level or the inclusion of CSLs have different effects on θ and Θ, depending on the phase. For the GL phase, θ is essentially insensitive to the environmental conditions. Although Θ evidences somewhat larger variations (range 15°–21°), these changes are largely non-systematic and may arise from insufficient convergence. For the LC phase, Θ is low and largely insensitive to the environmental conditions, whereas θ nearly systematically increases upon reducing the hydration level or increasing the concentration of TRH, or, to a larger extent, MET. This is likely due to the lateral expansion of the bilayer increasing the mismatch between effective headgroup and tail cross-sections, and thus, the requirement for tilting or kinking to achieve optimal packing of the chain. In summary, θ is positively correlated with a_{xy}, whereas Θ is only weakly sensitive to the environmental conditions for a given phase. The correlation between area per lipid and tilting behavior is further explored in a companion article (Laner et al. 2014).

Finally, the phase-assignment descriptor η of Eq. 1 successfully ascribes nearly all the trajectory configurations sampled along the 18 equilibrium simulations to one of the two phases (GL or LC), with occurrences of at least 99.9% in all cases.

Concerning the H-bonding properties (Table 3), the main observations in the absence of CSL (system P_N) are that (Laner et al. 2013): (1) the occurrence of inter-layer lipid-lipid H-bonds ($2n_L^{-1}N_{LL}^{inter}$) is limited, increases with decreasing hydration, and is systematically higher for the

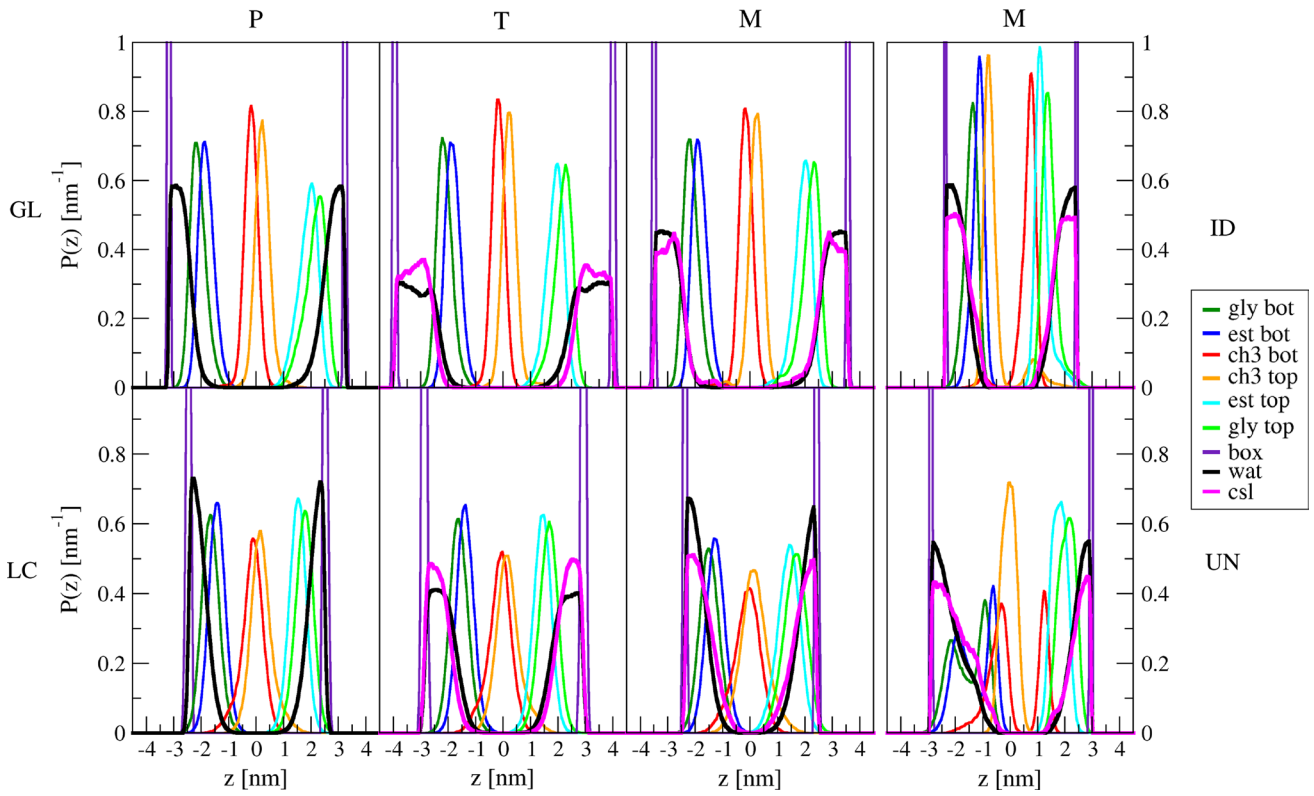

Fig. 3 Probability distribution profiles of different atoms along the bilayer normal calculated over a subset of the simulations. The six *panels* on the left correspond to simulations under equilibrium conditions for the different CSLs (P, T, or M) at full hydration (F) and at low concentration for MET (M_L), initiated either from a structure appropriate for the GL phase and carried out at 318 (P,T) or 302 (M) K, or from a structure appropriate for the LC phase and carried out at 338 K, i.e., simulations $P_NF_{GL}318$, $P_NF_{LC}338$, $T_NF_{GL}318$, $T_NF_{LC}338$, $M_LF_{GL}302$ and $M_LF_{LC}338$. The two *panels* on the right are examples of occurrence of an ID phase or of UN configurations in the presence of MET, corresponding to the end of simulations $M_MF_{LC}302$ and $M_LF_{LC}302$, respectively. The atoms considered for the distributions are the glycerol oxygen atoms (gly), the ester oxygen atoms (est), the terminal methyl groups (ch3), the water oxygen atoms (wat), and the CSL oxygen atoms (csl). For lipid atoms, a distinction is made between lipids belonging to the bottom (bot) and top (top) leaflets. The distributions of the box-wall position (box) are also shown. The profiles are normalized to one, centered at the bilayer midplane and evaluated using a histogram bin width of 0.05 nm. The data is averaged over the last 24 ns of the simulations. The simulation labels and conditions are summarized in Table 1

LC compared to the GL phase; (2) the occurrence of intra-layer lipid-lipid H-bonds ($2n_L^{-1}N_{LL}^{intra}$) is about 2.0 per lipid for the GL phase and about 1.4 per lipid for the LC phase, essentially independent of the hydration level; (3) the occurrence of lipid-water H-bonds ($n_L^{-1}N_{LW}$) is about 1.8–2.2 per lipid for the GL phase and about 2.2–2.8 per lipid for the LC phase, and decreases with decreasing hydration; (4) the total number of H-bonds per lipid (N_L^{tot}) is essentially independent of the phase and hydration level, with a value close to four (4.1–4.3).

For the inter-layer lipid-lipid H-bonds, the trends in the absence of CSL can easily be rationalized based on the average distance between periodic copies of the bilayers in the simulations, and considering the higher fluidity and temperature of the bilayer in the LC phase compared to the GL phase (Laner et al. 2013). In the presence of CSLs, the occurrences of these H-bonds are reduced to nearly zero, suggesting that the CSLs damp the fluctuations of the headgroup positions along the bilayer normal. To our knowledge, there is no direct experimental information available concerning transient H-bonding between stacked bilayers, which could occur e.g., in multilamellar (Yamazaki et al. 1992) or stacked monolamellar (Ariga et al. 2006) vesicles. However, H-bonds between headgroups from opposing (water-separated) leaflets have been mentioned as a possible source of attractive interaction between bilayers in the context of oligopeptide-carrying lipids (Ariga et al. 2006), phospholipids (McIntosh 2000) and cerebrosides (Kulkarni et al. 1999).

For the intra-layer lipid-lipid H-bonds, the higher occurrence in the GL compared to the LC phase can easily be rationalized based on the higher extent of ordering and the smaller area per lipid in the former phase (Laner et al. 2013). The CSLs do not significantly affect the occurrences of these H-bonds in the GL phase, and in the case of TRH, in the LC phase. However, the corresponding

occurrences for the LC phase are reduced in the presence of MET, and decrease further upon increasing the CSL concentration.

For the lipid-water H-bonds, the lower occurrences in the GL compared to the LC phase can again easily be rationalized based on the lower extent of ordering (increased exposure of the headgroups to the solvent) and the larger area per lipid of the latter phase, while the decrease with decreasing hydration level is directly related to the availability of water in the system (Laner et al. 2013). The CSLs systematically reduce the occurrences of these H-bonds in both the GL and the LC phases. However, they also introduce new lipid-CSL H-bonds ($n_{\mathrm{L}}^{-1}N_{\mathrm{LC}}$) in both phases. Expectedly, the occurrences of these new H-bonds increase upon increasing the CSL-to-water ratio in the system.

When considering the sum $N_{\mathrm{L}}^{\mathrm{tot}}$ of the inter-layer lipid-lipid, intra-layer lipid-lipid, lipid-water and lipid-CSL H-bonds per lipid, this number remains essentially constant for all the systems considered, with a value close to four (3.9–4.3). In the absence of CSL, the lipid-water H-bond deficit caused by lowering the hydration is compensated for by an increase in the number of (mainly inter-layer) lipid-lipid H-bonds (Laner et al. 2013). In the presence of CSLs, one essentially observes a suppression of inter-layer lipid-lipid H-bonds, nearly no changes in intra-layer lipid-lipid H-bonds (except for the LC phase in the presence of MET, where this number decreases) and a partial substitution of lipid-water by lipid-CSL H-bonds. However, in both cases, the total number of H-bonds per lipid, i.e., the H-bond saturation of the bilayer headgroups, is nearly unaffected. Such a nearly quantitative compensation effect between changes in the numbers of lipid-lipid and lipid-environment H-bonds upon altering the phase or environment of a bilayer, i.e., the conservation of the headgroup H-bond saturation, has been observed previously for this system (Horta et al. 2010b; Laner et al. 2013), as well as in different contexts (Pereira et al. 2004; Pereira and Hünenberger 2006, 2008a, b; Horta et al. 2010a). Given this conservation principle, a change in the bilayer environment can be viewed as inducing a mere redistribution of the four

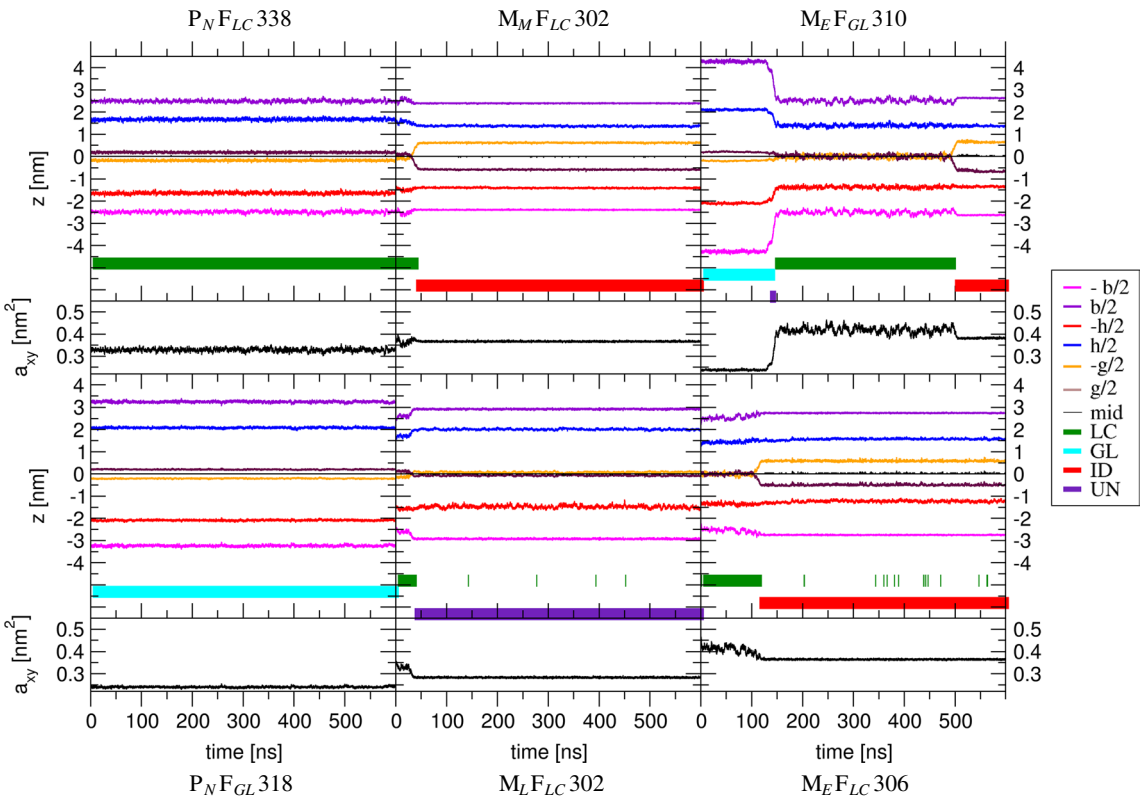

Fig. 4 Time series of the bilayer structural properties calculated over a subset of simulations. The two *panels* on the left correspond to simulations in the absence of CSL and at full hydration, initiated either from the GL phase and carried out at 318 K or from the LC phase and carried out at 338 K. They present no phase transition. The four *panels* on the right correspond to simulations in the presence of MET at full hydration, and presenting the occurrence of an ID phase or of UN configurations. The quantities displayed are the area per lipid a_{xy}, the assigned phase (η, see Eq. 1; LC, GL, ID, or UN), the box dimension ($-b/2$, $b/2$), the leaflet extension ($-h/2$, $h/2$) and the position of the tail methyl plane ($-g/2$, $g/2$) along the z-axis and the bilayer mid-plane (mid; average position of the tail methyl groups of both leaflets, set to $z = 0$ by construction). The simulation labels and conditions are summarized in Table 1

lipid-environment H-bonds among the different species present in the system, as illustrated in Fig. 2.

In the available X-ray structures of pure monoglycerides (no water) in the crystalline phase (Larsson 1966; Goto and Takiguchi 1985; Goto et al. 1988), the free glycerol hydroxyl groups are each involved in two lipid-lipid H-bonds, one inter-layer and one intra-layer. The partitioning of the four H-bonds is thus 50 % intra-layer and 50 % inter-layer. For the GL phase, the results in the absence of CSL suggest that the inter-layer H-bonds observed in these crystals are replaced by lipid-water H-bonds essentially on a one-to-one basis, as previously suggested (Pezron et al. 1990). For the LC phase at full and half hydration, the results suggest that, in addition, about 15 % of the H-bonds observed in these crystals are replaced by lipid-water H-bonds as well, resulting from the temperature increase, the higher inherent extent of disorder in the LC phase and the larger area per lipid.

For the GL phase, the substitution in the presence of CSLs remains similar, i.e., the inter-layer H-bonds observed in the crystals are replaced by lipid-environment (i.e., lipid-water or lipid-CSL) H-bonds, essentially on a one-to-one basis. For the LC phase, the extra substitution of a fraction of the H-bonds observed in the crystals by lipid-environment H-bonds also amounts to about 15 %, except in the presence of MET, where it rises to 20–30 %, increasing with the CSL concentration.

The relative strengths of the H-bonds between pairs of species in the systems, as qualitatively probed by the average hydrogen-acceptor distance and donor-hydrogen-acceptor angle (a smaller distance and an angle closer to 180° implying a stronger bond) are, in decreasing order: GMP-MET > GMP-GMP > GMP-water > GMP-TRH. The higher strength of the GMP-MET relative to the GMP-TRH H-bonds is due to the different penetration depths (deeper for MET) and relative sizes (larger for TRH, leading to suboptimal H-bond geometries) of the two molecules.

A H-bond conservation principle similar to that suggested for the lipid headgroups also holds for the CSL and water molecules. The total number of H-bonds per CSL molecule (N_C^{tot}) is close to 2.2 for MET (range 2.1–2.4) and 14.0 for TRH (range 12.6–14.4) for all systems. The different numbers are related to the number of potentially H-bonding groups per molecule. The total number of H-bonds per water molecule (N_W^{tot}) is close to 3.0 (range 2.9–3.3) for all systems.

The distribution profiles $P(z)$ of the different atoms along the bilayer normal (Fig. 3; six panels on the left) reveal a clear double-leaflet structure for the equilibrium simulations considered here. The profiles are narrower for the GL compared to the LC phase (smaller d_z; see above). The tail methyl groups from the bottom and top leaflets present well-resolved distributions with significant overlap and the expected ordering in terms of peak positions (bottom below top), the distributions being slightly broader and the overlap more pronounced in the LC compared to the GL phase. Note that the overlap does not result from a partial interdigitation of the tail ends, but from different offsets in the methyl-methyl contact points of opposite lipid pairs along the z-axis (variations among lipid pairs and fluctuations in time). As expected, the glycerol atom distributions are closer to the leaflet surfaces than the ester distributions.

For the systems without CSL, water penetrates the bilayer up to the ester region and presents a large overlap with the glycerol region, especially in the LC phase. The same applies to the two types of CSLs. However, comparatively, TRH presents a more limited overlap with the lipid headgroups compared to MET. This difference is more pronounced in the LC phase and is easily understood when considering the very different sizes of the two types of molecules. Another difference is the relative extent of penetration of the two CSLs compared to water (Pereira and Hünenberger 2008a; Horta et al. 2010a). For TRH, in both the GL and LC phases, the CSL penetrates the bilayer less deeply than water, thereby forming a surface coating layer. For MET in the LC phase, the opposite trend is observed, suggesting a preferential affinity of the bilayer surface for the CSL compared to water, especially in the ester region. A more detailed interpretation of these differences is given in Pereira and Hünenberger (2008a).

Differences between water, TRH and MET are also seen in the extent of H-bonded bridging (Table 4), i.e., the number of water molecules n_W^m and CSL molecules n_C^m being simultaneously H-bonded with a given number m of lipid molecules. The quantities $n_L^{-1}(n_W - n_W^o)$ and $n_L^{-1}(n_C - n_C^o)$ represent average numbers of water and CSL molecules, respectively, H-bonded to the bilayer on a per-lipid basis. For all systems, these numbers are systematically lower for the GL compared to the LC phase. In the absence of CSLs, the average number of H-bonded water molecules ranges between 1.2 and 2.2, and decreases with decreasing hydration level. In the presence of TRH, the average numbers of H-bonded water and CSL molecules are in the ranges of 0.6–1.7 and 0.2–0.4, respectively. In the presence of MET, the corresponding numbers are in the ranges of 1.0–2.1 and 0.2–0.6, respectively. Expectedly, the number of bound water molecules decreases and the number of bound CSL molecules increases upon increasing the CSL concentration.

The quantities $(n_W - n_W^o)^{-1} n_W^m$ and $(n_C - n_C^o)^{-1} n_C^m$ represent fractions of these H-bonded water and CSL molecules, respectively, forming simultaneously H-bonds with (i.e., bridging) m lipids. Considering the H-bonded water molecules in the absence of CSL and at full hydration, about 70 % are H-bonded to a single lipid, about 25 % to two lipids simultaneously, and about 5 % to three lipids

Table 5 Average dynamic properties calculated from a subset of simulations corresponding to equilibrium conditions

Simulation	D_{xy} [10^{-11} m^2 s^{-1}]	τ_1^R [ns]	c_1^R	τ_2^R [ns]	c_2^R	τ_1^W [ns]	c_1^W	τ_2^W [ns]	c_2^W
$P_NF_{GL}318$	2.99	0.18	0.22	0.76	0.04	10.96	0.97	82.04	0.95
$P_NF_{LC}338$	13.77	0.12	0.10	3.10	0.06	1.25	0.81	6.78	0.66
$P_NH_{GL}318$	1.53	0.19	0.23	0.90	0.05	17.38	0.98	249.05	0.97
$P_NH_{LC}338$	11.63	0.13	0.13	2.33	0.06	1.30	0.82	5.56	0.64
$P_NQ_{GL}318$	1.14	0.23	0.29	0.81	0.06	18.78	0.98	229.17	0.97
$P_NQ_{LC}338$	8.45	0.15	0.17	1.65	0.06	1.41	0.83	5.42	0.65
$T_NF_{GL}318$	1.18	0.25	0.31	0.83	0.06	19.61	0.98	109.08	0.97
$T_NF_{LC}338$	7.80	0.15	0.17	1.32	0.05	1.80	0.86	5.59	0.69
$T_NH_{GL}318$	0.73	0.31	0.38	1.00	0.10	32.16	0.99	203.81	0.98
$T_NH_{LC}338$	4.63	0.20	0.26	0.98	0.06	2.21	0.89	5.99	0.72
$T_NQ_{GL}318$	0.34	0.44	0.48	1.71	0.22	33.02	0.99	195.45	0.98
$T_NQ_{LC}338$	2.57	0.29	0.37	1.00	0.10	2.80	0.91	6.90	0.75
$M_LF_{GL}302$	1.18	0.31	0.38	0.85	0.08	31.53	0.99	261.85	0.98
$M_LF_{LC}338$	14.63	0.11	0.10	2.31	0.05	1.25	0.81	5.02	0.62
$M_MF_{GL}302$	1.33	0.30	0.38	0.78	0.08	18.80	0.98	95.15	0.97
$M_MF_{LC}338$	18.13	0.11	0.09	3.39	0.05	1.14	0.80	4.19	0.58
$M_EF_{GL}306$	2.29	0.29	0.36	0.81	0.08	18.51	0.98	76.52	0.97
$M_EF_{LC}338$	19.38	0.10	0.08	2.27	0.04	1.00	0.77	3.38	0.53
$M_MF_{LC}302$	1.25	0.28	0.36	1.05	0.10	14.90	0.98	59.70	0.96

This subset corresponds to the simulations started from a structure appropriate for the GL phase at reference temperature $T = 302$ (systems M_L and M_M), 306 (system M_E) or 318 K (all other systems), as well as from a structure appropriate for the LC phase at reference temperature $T = 338$ K, for the different CSLs (P, T or M), numbers of CSL molecules (N, L, M or E) and hydration levels (F, H or Q). As an example for the ID phase, the values for simulation $M_MF_{LC}302$ are also provided (last line). The quantities reported are the lipid lateral diffusion coefficient D_{xy}, the first (τ_1^R) and second (τ_2^R) relaxation times corresponding to the two observed decays in the rotational motion with corresponding residual correlations (c_1^R and c_2^R), and the first (τ_1^W) and second (τ_2^W) relaxation times corresponding to the two observed decays in the wobbling motion with corresponding residual correlations (c_1^W and c_2^W). The data is calculated over the last 24 ns of simulation. The simulation labels and conditions are summarized in Table 1. Corresponding data for the entire set of 83 simulations can be found in Tables S.11–S.13 of the Supplementary Material document

simultaneously, irrespective of the phase. Upon decreasing the hydration level, the extent of H-bonded bridging by water tendentially increases in both phases. Addition of TRH at full hydration slightly increases the extent of water bridging in the GL phase, with little effect in the LC phase. Addition of MET at low concentration has little effect on the extent of water bridging in both phases. Upon increasing the CSL concentration, water bridging is slightly enhanced in the GL phase and decreased in the LC phase, most likely due to the lateral expansion of the bilayer.

Considering the bound TRH molecules, the extent of bridging is about the same in the GL and LC phases, and tendentially increases with decreasing hydration. Simultaneous H-bonding of one TRH molecule with up to eight different lipid molecules can be observed, albeit very infrequently [see Fig. 6 in Pereira and Hünenberger (2008a)]. However, H-bonding with two, three, four or five lipids is frequent (about 30, 20, 10 and 5%, respectively, of the bound TRH molecules). For the bound MET molecules, H-bonding to more than two lipids simultaneously is scarce. The extent of bridging is overall lower in the LC than in the GL phase, and tendentially decreases with increasing MET content. This is likely due to higher fluidity and disorder in the LC phase. This difference between MET and TRH in the extent of H-bonded bridging of the lipids is not unexpected, considering the different sizes and number of H-bonding groups of the two molecules, and their tight interaction with the membrane surface as revealed by the distribution profiles (Fig. 3). The observation that TRH forms a coating layer and a H-bonding network with the lipids at the surface of the bilayer has been reported previously (Pereira et al. 2004; Pereira and Hünenberger 2006, 2008a; Horta et al. 2010a), and forms the basis of the headgroup-bridging hypothesis for anhydrobiotic membrane stabilization by TRH.

Concerning the dynamic properties (Table 5), the main observations in the absence of CSL are that (Laner et al. 2013): (1) the translational diffusion coefficient D_{xy} is systematically lower for the GL phase compared to the LC phase (factor 4–8); (2) it decreases with decreasing

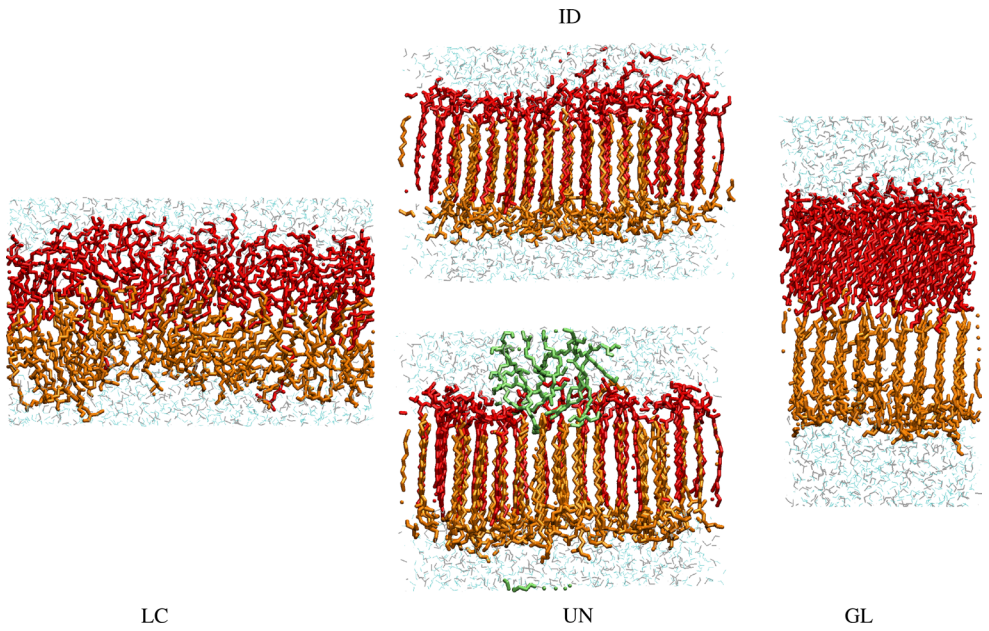

Fig. 5 Illustrative structures corresponding to the different phases of the GMP lipid bilayer. Shown are snapshots illustrating the three phases LC (at 240 ns), GL (at 60 ns) and ID (at 600 ns) occurring in simulations $M_EF_{GL}310$, as well as the configurations UN occurring in simulation $M_LF_{LC}302$ (at 500 ns). Lipids are colored in *orange* and *red* to indicate the two different leaflets (bottom and top), MET is displayed in *grey*, and water molecules are displayed in *light blue*. The lipids shown in *green* in the UN configuration are extruded from the top leaflet. Note that the structures for GL and LC are shown along the *x*-axis of the box, while the structures for ID and UN were rotated around the *z*-axis to highlight their structural characteristics (interdigitation and alignment). The simulation labels and conditions are summarized in Table 1

hydration level for the two phases; (3) the first decay time τ_1^R for the rotational autocorrelation function, attributed to the rotation of a single lipid around its axis and associated with a low residual correlation (as expected for a vector that samples the accessible space isotropically), corresponds to a timescale of about 0.2 ns for the GL phase and 0.1 ns for the LC phase; (4) the first decay time τ_1^W for the wobbling autocorrelation function, attributed to the wobbling of a single lipid and associated with a high residual correlation (as expected for a vector that does not sample the accessible space isotropically), corresponds to a timescale of about 10–20 ns for the GL phase and 1.5 ns for the LC phase.

For the translational diffusion, the trends in the absence of CSL could easily be rationalized (Horta et al. 2010b; Laner et al. 2013) based on the lower extent of ordering of the LC phase compared to the GL phase, but may also reflect in part the higher simulation temperature. The reduction of the lateral mobility upon dehydration is probably related to the slightly higher viscosity of confined water (Raviv et al. 2001) and the formation of a small amount of inter-layer H-bonds across periodic boundaries (Table 3). Comparison of the present estimate of 13.8×10^{-11} $m^2\ s^{-1}$ for GMP in the LC phase at full hydration with the experimental (Vaz et al. 1985) and simulation (Klauda et al. 2006) values of 1.25 and 0.95×10^{-11} $m^2\ s^{-1}$, respectively, for DPPC at 50 °C indicates that the lateral diffusion of GMP molecules (single acyl chain and low polarity headgroup) is much faster than that of DPPC (two acyl chains and zwitterionic headgroup).

The inclusion of the two CSLs considered has opposite effects on the dynamic properties. In the presence of TRH, the value of D_{xy} is decreased and the rotational and wobbling motions are also slowed down (longer τ_1^R and τ_1^W) for both the GL and the LC phases. In the presence of MET, the value of D_{xy} is increased and the rotational and wobbling motions slightly accelerated (shorter τ_1^R and τ_1^W) for the LC phase, with little effect for the GL phase. In the case of TRH, the damping of the lipid dynamics in both phases probably results from the high extent of H-bonded headgroup bridging by the sugar molecules (see above), which leads to a restriction in the lipid motions. In the case of MET, the acceleration of the lipid dynamics in the LC phase is probably correlated with the increase in the area per lipid.

Interdigitated phase

The 18 equilibrium simulations discussed in the previous section are initiated from either the GL or the LC phase, and do not present phase transitions at the temperatures considered. Most of the remaining 65 simulations carried

out at intermediate temperatures, which will be discussed in details in the next two sections, evidence no or a single GL→LC or LC→GL transition over the 600 ns time period.

As illustrated in Fig. 4, there are four exceptions in which the sampling of another phase is observed in the presence of MET. These are simulations $M_LF_{LC}302$ (LC→UN at 30 ns), $M_MF_{LC}302$ (LC→ID at 40 ns), $M_EF_{LC}306$ (LC→ID at 115 ns) and $M_EF_{GL}310$ (GL→LC at 140 ns followed by LC→ID at 500 ns). Illustrative structures for the LC, GL and ID phases, as well as for the unrecognized UN configurations, are shown in Fig. 5. The average values of key properties calculated over the last 24 ns of simulation $M_MF_{LC}302$ (ID phase) are reported as last lines in Tables 2, 3, 4 and 5. Distribution profiles calculated over the last 24 ns of simulations $M_MF_{LC}302$ (ID phase) and $M_LF_{LC}302$ (UN configurations) are also shown in Fig. 3.

The ID phase, occurring in simulations $M_MF_{LC}302$, $M_EF_{LC}306$ and $M_EF_{GL}310$, is interdigitated. The UN configurations, occurring in simulation $M_LF_{LC}302$, also belong to the ID phase. However, some lipids of one leaflet are extruded (tails exposed to water, see distribution profile in the bottom right panel of Fig. 3 and an illustrative structure in Fig. 5), which prevents it from being recognized as ID by the phase-assignment descriptor η of Eq. 1. Note that in other simulations, a transient assignment to UN generally indicates instead that the system is in an intermediate state between GL and LC. This simulation $M_LF_{LC}302$ will not be further discussed.

Interdigitation is another possibility besides single-lipid (LC) or collective (GL) chain tilting to remedy the mismatch between the headgroup and tail cross-sections of the lipids. In the ID phase, the bottom and top leaflets overlap over a length of about 13 carbon atoms along the opposing chains. In Fig. 3, the upper right panel shows the ID phase with the tail methyl groups clearly penetrating the opposite leaflet. As a result of this interpenetration, the distance g between the terminal methyl planes of the bottom and top leaflets (bottom to top) is negative (about −1.2 nm). The area per lipid a_{xy} is about 0.37 nm^2, larger than the value for the LC phase in the absence of CSL (about 0.31 nm^2) and comparable to the corresponding value in the presence of MET at low concentration (system M_L). The bilayer thickness d_z is about 2.3 nm, smaller than the value for the LC phase in the absence of CSL (about 3.1 nm) and comparable to the corresponding value in the presence of MET at elevated concentration (system M_E). The volume per lipid v_{xyd} is about 0.41 nm^3 and the chain-averaged order parameter S_{chn} about 0.41, the lowest and highest values, respectively, observed in the entire set of simulation. The corresponding effective volume per methylene group in the bilayer interior is 0.025 nm^3, identical to the corresponding estimate for solid alkanes (Small 1984). The single-lipid and collective tilt angles θ and Θ are about 10° and 4°, respectively, indicating that the chains are essentially aligned along the bilayer normal. In terms of H-bonding and H-bonded bridging properties, the ID phase is intermediate between the GL and LC phases. For the dynamic properties, the values are similar to the GL phase.

In summary, the ID phase is characterized by: (1) the interdigitations of the lipids; (2) the absence of significant tilting, at both the single-lipid and collective levels; (3) a strong lateral expansion and transverse compactness compared to the LC phase, and, to an even higher extent, the GL phase; (4) a high tail packing density and chain ordering (predominance of all-*trans* conformations) compared to the GL phase, and, to an even higher extent, the LC phase; (5) a low fluidity comparable to that of the GL phase. Note that the order parameters for the ID phase (chain average of about 0.41) are even higher than those for the GL phase (about 0.31), as observed experimentally for other lipids (Boggs and Rangaraj 1985). It should be recalled, however, that conformational disorder in the tails and chain tilting relative to the bilayer normal both contribute to decreasing the order parameters of the lipids (Douliez et al. 1998). Consequently, the order parameter increase from GL to ID results in principle from both the tighter chain packing and the suppression of the tilting. The relative influence of these two components is further discussed in a companion article (Laner et al. 2014).

In the present simulations, the ID phase is observed only in systems containing MET and is only reached from the LC phase, never directly from the GL phase. This is consistent with the experimental finding that the ID phase of DPPC occurs in the presence of alcohols but not in pure-lipid systems (Rowe and Campion 1994; Wang and Dea 2009; Griffin et al. 2010; Wanderlingh et al. 2010; Kurniawan et al. 2012), as also observed in coarse-grained simulations of phosphatidylcholines (Venturoli et al. 2006). To our knowledge, only one simulation study revealed an ID phase in the absence of alcohols (Klauda et al. 2006) (probably an artifact of approximate electrostatics), and only one simulation study of distearoylphosphatidylethanolamine (DSPE) presented a direct GL→ID transition (Quin et al. 2009).

Phase transitions

To characterize the influence of the presence and concentration of CSLs on the phase-transition properties of the bilayer, the complete set of 83 simulations is now considered (Table 1). The time series of the area per lipid a_{xy}, the chain-averaged order parameter S_{chn}, and the bilayer thickness d_z are displayed in Fig. 6 for all simulations.

As already mentioned in the previous section, most of the simulations evidence no or a single GL→LC or LC→GL

transition over the 600 ns time period. Trajectory segments corresponding to either of these two phases can be identified by their values of a_{xy} (about 0.24 or 0.31 nm^2 for GL and LC, respectively), S_{chn} (about 0.31 or 0.17), and d_z (about 3.8 or 3.2 nm). Occurrences of the ID phase in three simulations can be identified by corresponding values of 0.37 nm^2, 0.41 and 2.3 nm, respectively. Expectedly, the trajectory segments corresponding to a LC phase present larger fluctuations of the three quantities monitored compared to those corresponding to a GL or ID phase. The occurrence of a possible single transition between two of these three phases in the different simulations is summarized in Table 6. The only special cases are simulation $\mathrm{M_E F_{GL}}310$, where two successive transitions are observed (GL→LC at 140 ns followed by LC→ID at 500 ns), and simulation $\mathrm{M_L F_{LC}}302$, which presents unassigned ID-like configurations (LC→UN at 40 ns).

Considering the system $\mathrm{P_N}$, the simulations initiated from a GL structure and carried out at temperatures of at least 322 (F and H) or 326 (Q) K undergo a transition to the LC phase, the other ones remaining in the GL phase. At the three hydration levels, the simulations initiated from a LC structure remain in the LC phase at 338 K. However, the corresponding simulations at 318 K do not undergo a transition to the GL phase within 600 ns. The absence of transition to the GL phase at this temperature is not viewed as incompatible with T_m values on the order of 320–324 K, considering the expected long timescale of a LC→GL transition with such a small temperature difference to T_m (Horta et al. 2010b; Laner et al. 2013). The relationship between transition kinetics and temperature relative to T_m is further discussed in a companion article (Laner and Hünenberger 2014b). Note that even in the absence of a transition, the area per lipid is noticeably lower in these simulations compared to the corresponding simulations at 338 K. The above results lead to suggested transition temperatures T_m of 320 ± 2 (F), 320 ± 2 (H) and 324 ± 2 (Q) K for the system $\mathrm{P_N}$ at full, half and quarter hydration, respectively. These estimates are all within at most 7 K of the T_m values inferred from the experimental phase diagram of the GMP-water system (Krog and Larsson 1968; Horta et al. 2010b), namely 323, 326, and 331 K.

For the system $\mathrm{T_N}$, the phase transitions occur at the same temperatures. Here, a shift to lower transition temperatures was initially expected, considering that TRH is experimentally found to counteract the T_m increase in pure bilayers upon decreasing hydration (Tunnacliffe et al. 2001; Tunnacliffe and Lapinski 2003; Crowe et al. 2005; Adams et al. 2007; Albertorio et al. 2007; Hengherr et al. 2008; Zhmakin 2008). However, the concentrations

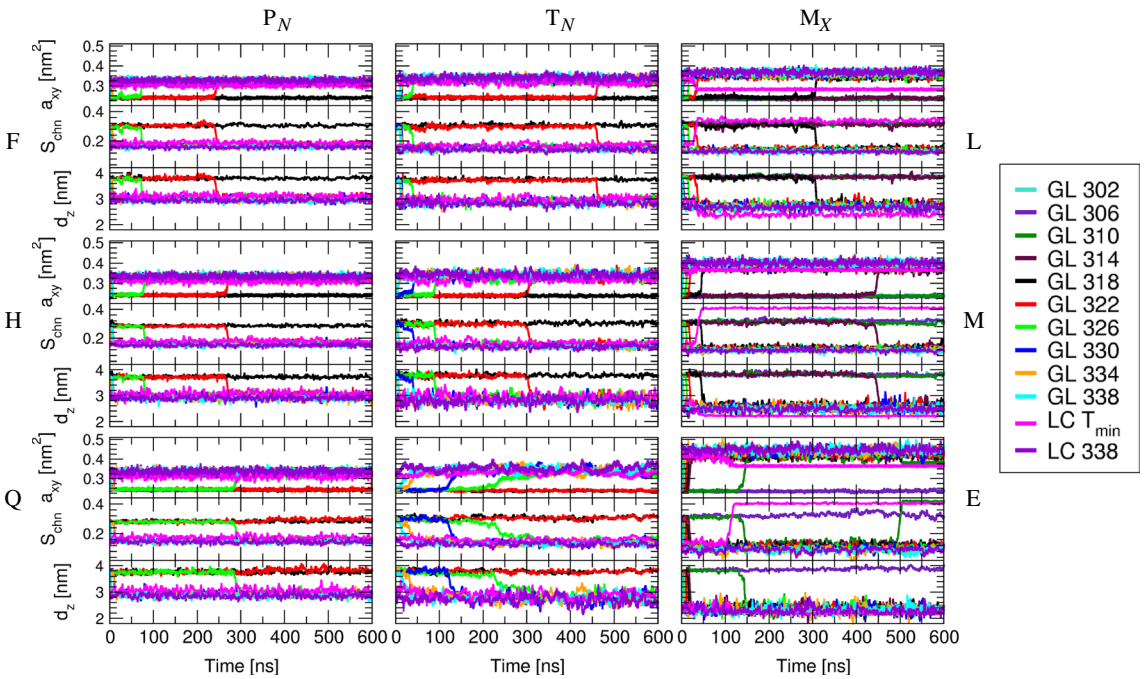

Fig. 6 Time series of structural properties along the different simulations. The quantities displayed are the area per lipid a_{xy}, the chain averaged order parameter S_{chn} and the bilayer thickness d_z. The simulations differ by the different CSLs (P, T or M), numbers of CSL molecules (N, L, M, or E) and hydration level (F, H or Q). They were started from a structure appropriate for the GL phase and carried out at reference temperatures ranging from $T_{\mathrm{min}} = 302$ (systems $\mathrm{M_L}$ and $\mathrm{M_M}$), 306 (system $\mathrm{M_E}$) or 318 K (all other systems) to 338 K, or from a structure appropriate for the LC phase and carried out at reference temperatures T_{min} or 338 K. The simulation labels and conditions are summarized in Table 1

Table 6 Possible occurrence of a phase transition during the different simulations

T [K]	P_N			T_N			M		
	F	H	Q	F	H	Q	L	M	E
302							–	–	
306							–	–	–
310							–	–	◊
314							–	×	×
318	–	–	–	–	–	–	×	×	×
322	×	×	–	×	×	–	×	×	×
326	×	×	×	×	×	×	×	×	×
330	×	×	×	×	×	×	×	×	×
334	×	×	×	×	×	×	×	×	×
338	×	×	×	×	×	×	×	×	×
LC T_{min}	–	–	–	–	–	–	□	◊	◊
LC338	–	–	–	–	–	–	–	–	–

The simulations were started from a structure appropriate for the GL phase and carried out at reference temperatures ranging between T_{min} = 302 (systems M_L and M_M), 306 (system M_E) or 318 K (all other systems) and 338 K, or from a structure appropriate for the LC phase and carried out at reference temperatures T_{min} or 338 K. They differ by the different CSLs (P, T or M), numbers of CSL molecules (N, L, M, or E) and hydration levels (F, H or Q). A minus (–) indicates the absence of a transition, a cross (×) the presence of a GL→LC or LC→GL transition (depending on the starting configuration), a diamond (◊) the presence of a LC→ID transition, and a square (□) the presence of a LC→UN transition. All simulations present at most one transition, except $M_EF_{GL}310$, which undergoes a transition to LC followed by a transition to ID. See Table 1 for the simulation labels and conditions

considered in the present study (42.9 % w/w TRH-to-lipid) might be too low to see a pronounced effect. For comparison, the TRH content used in experiments can be up to 1:1 (Tsvetkova et al. 1998) or 5:1 (Ricker et al. 2003) w/w TRH-to-lipid.

The systems M_X (X = L, M, or E) evidence a lowering of the transition temperature in comparison to the previous systems, increasingly pronounced upon increasing the MET concentration. The simulations initiated from a GL structure and carried out at temperatures of at least 318 (L), 314 (M) or 310 (E) K undergo a transition to the LC phase, although the simulation M_E at 310 K presents a subsequent transition to the ID phase. At the three concentrations, the simulation started from a LC structure and carried out at 338 K remains in the LC phase, whereas the simulation started from a LC structure and carried out at T_{min} (302, 306 or 310 K) undergoes a LC→ID transition (UN configurations being considered as a form of ID phase). These results lead to suggested transition temperatures of 316 ± 2 (L), 312 ± 2 (M), and 308 ± 2 (E) K for the M_X systems. This is in line with the concentration-dependent T_m decrease induced experimentally by short-chain aliphatic alcohols at moderate concentrations (Rowe 1983, 1985; Löbbecke and Cevc 1995; Rosser et al. 1999), i.e., before the biphasic reversal takes place. In this regime, the GL phase (rather than the ID phase) should be the thermodynamically most stable ordered phase. However, the four simulations carried out at $T \leq 310$ K lead to the appearance of the ID phase instead. Furthermore, the ID phase is only reached in the simulations from the LC phase, i.e., no direct GL→ID transition was observed on the 600 ns timescale, the transition of simulation $M_EF_{GL}310$ being indirect (GL→LC→ID). This suggests that the GL phase might not be the thermodynamically most stable phase, but metastable instead. It is also in line with the observation that the MET concentrations considered in the simulations (7.8, 15.6 and 31.2 M for L, M, and E, respectively), are actually above the concentration at which the biphasic effect takes place experimentally (Rosser et al. 1999) for DPPC in the presence of MET, namely about 2.7 M. Clearly, more simulations are required to disentangle the thermodynamic and kinetic factors in interplay concerning the biphasic effect in the GMP system. This issue is addressed in a companion article (Laner and Hünenberger 2014a).

Temperature-dependent properties

The equilibrium phase properties at the extreme temperatures T_{min} (302, 306 or 318 K) and 338 K and the phase-transition temperatures inferred from the simulations have been discussed in the previous three sections. The present section completes the discussion by considering the temperature dependence of the phase properties between 318 and 338 K.

A number of the bilayer structural characteristics discussed in section "Equilibrium properties" are displayed as a function of the area per lipid a_{xy} in Fig. 7 as averages over the last 24 ns for the entire set of 83 simulations.

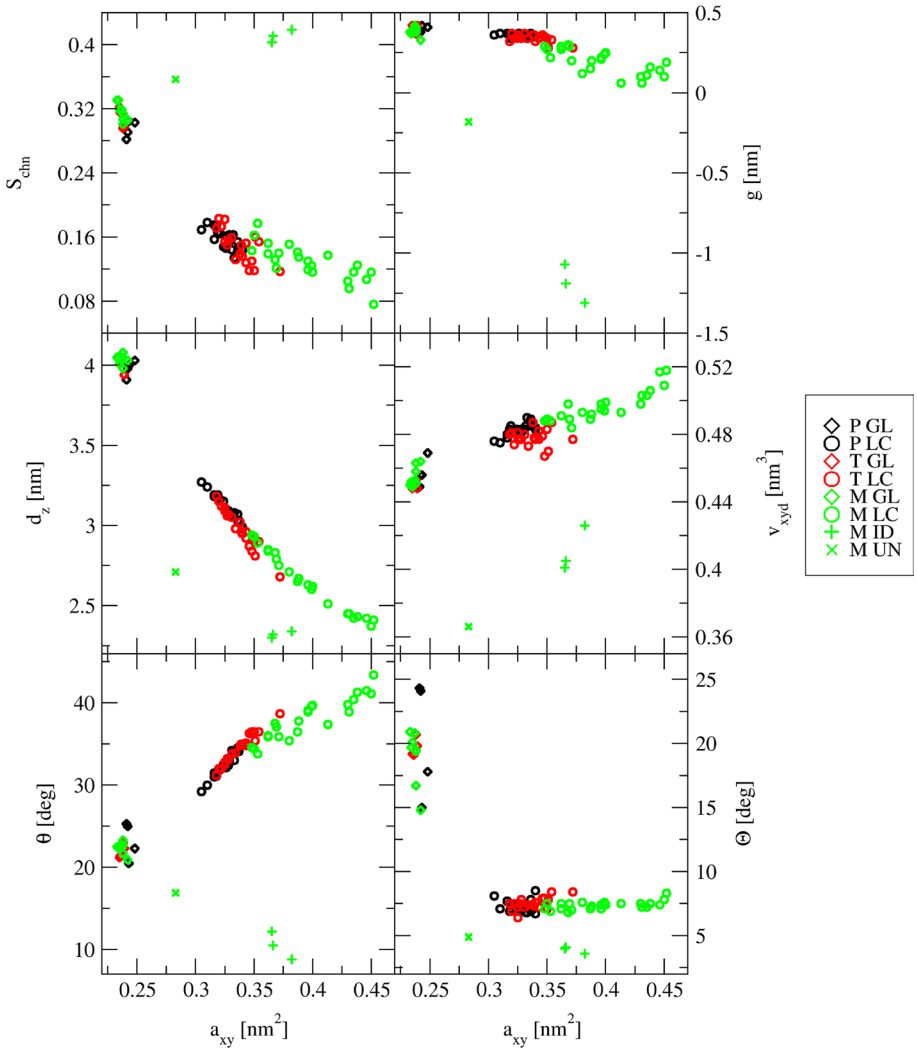

Fig. 7 Correlation between various structural parameters and the area per lipid for the entire set of simulations. Shown are correlation plots between the area per lipid a_{xy} and the chain-averaged order parameter S_{chn}, the average distance g between the terminal methyl planes of the two leaflets (top minus bottom), the bilayer thickness d_z, the volume per lipid v_{xyd}, the single-lipid tilt angle θ and the collective tilt angle Θ for the entire set of simulations. The values are averaged over the last 24 ns of the simulations. The simulations differ by the CSL (P, T or M) and the final phase of the simulation (LC, GL, ID of UN). The simulation labels and conditions are summarized in Table 1. The corresponding data can be found numerically in Tables S.5–S.7 of the Supplementary Material document

Considering the LC and GL phases together, most of the structural parameters are directly related to a_{xy}, being either negatively (S_{chn}, g, d_z) or positively (v_{xyd}, θ) correlated. These correlations also hold within the LC phase alone, whereas the GL phase evidences very little variations in a_{xy} . The only exception to this overall correlation pattern is the collective tilt angle Θ, which is sensitive to environmental variations in the GL phase (range 15°–25°) and essentially constant around 6.5° in the LC phase. This correlation between most observables and a_{xy} is truly remarkable in the sense that it does not seem to be significantly affected by other varying parameters (GL or LC phase, presence and concentration of a possible CSL, temperature). It is easily understood when one considers that a major thermodynamic driving force in lipid bilayers is the optimization of the chain packing within the bilayer interior. In effect, this strong driving force constrains d_z, θ and S_{chn} to be functions of a_{xy} at approximately constant v_{xyd}. However, Θ remains a free parameter accounting for the extent of correlation between lipids in the realization of a given θ value, the extent of this correlation having little influence on the chain packing density.

For the ID phase, the three data points (excluding UN) are insufficient to establish a trend as a function of a_{xy}. However, these points are clearly off relative to the correlations observed in the LC and GL phases, with anomalously high (S_{chn}) or low (g, which is now negative, as well as d_z, v_{xyd}, θ and Θ) values. Note, however, that if one correlates the parameters with $a_{xy}/2$ instead of a_{xy} for the ID phase, the ID points also approximately follow the correlation curves of the two other phases in terms of S_{chn}, v_{xyd} and θ.

The average values of the area per lipid a_{xy}, the chain-averaged order parameter S_{chn}, and the bilayer thickness d_z are displayed graphically as a function of temperature in Fig. 8 as averages over the last 24 ns for the entire set of 83 simulations. All the simulations can unambiguously be classified into three distinct groups with properties characteristic of a LC, GL or ID phase at the end of the simulation, except simulation $\mathrm{M_LF_{LC}302}$ leading to UN configurations. The LC and ID phases have comparable values for

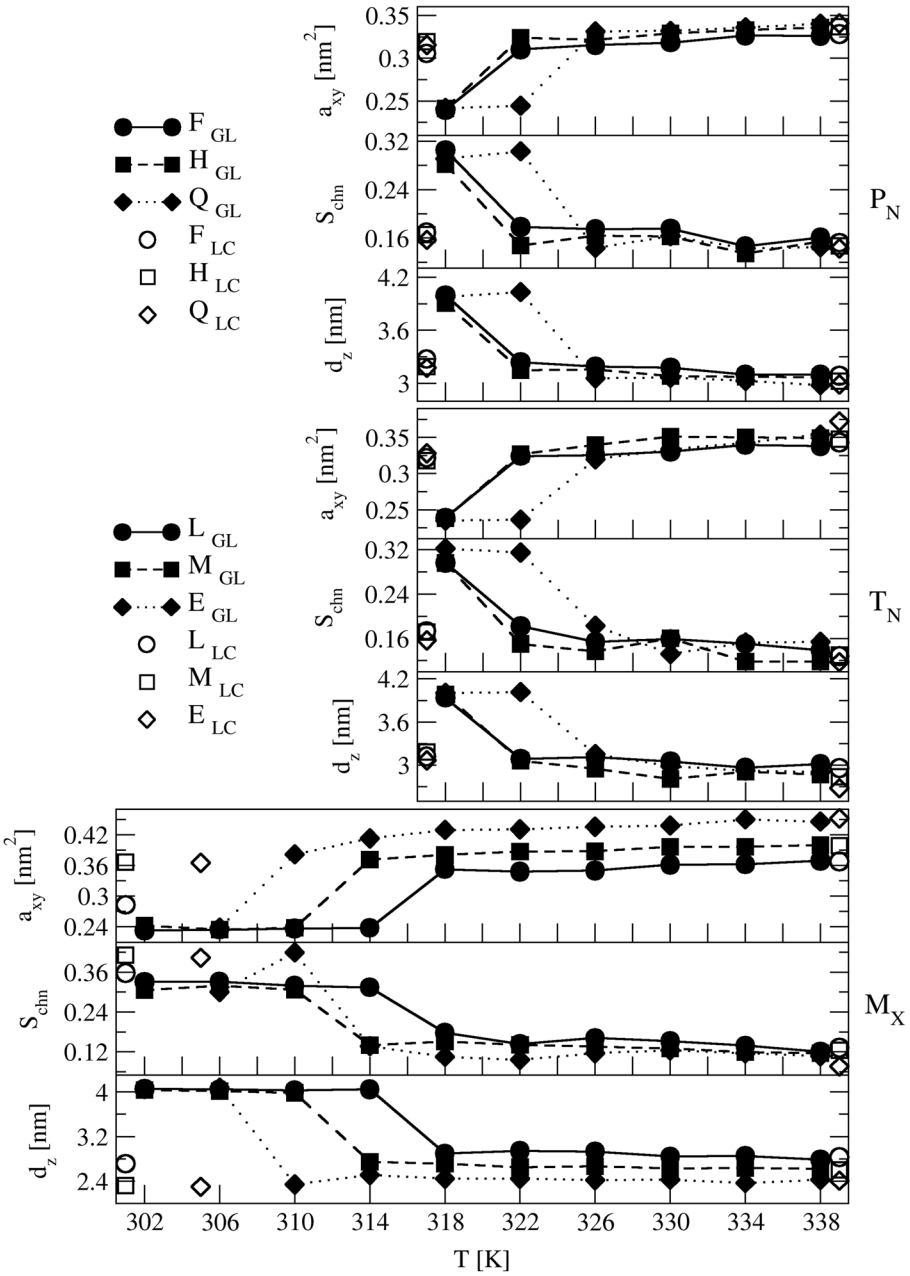

Fig. 8 Temperature dependence of the bilayer structural parameters for the entire set of simulations. Shown are the values of the area per lipid a_{xy}, the chain-averaged order parameter S_{chn} and the bilayer thickness d_z as a function of the simulation temperature. The simulations differ by the different CSLs (P, T or M), numbers of CSL molecules (N, L, M, or E) and hydration level (F, H or Q). They were started from a structure appropriate for the GL phase and carried out at reference temperatures ranging from $T_{\mathrm{min}} = 302$ (systems $\mathrm{M_L}$ and $\mathrm{M_M}$), 306 (system $\mathrm{M_E}$) or 318 K (all other systems) to 338 K in steps of 4 K, or from a structure appropriate for the LC phase and carried out at reference temperatures T_{min} or 338 K. The data is averaged over the last 24 ns of the simulation. Note that the LC points were slightly shifted to the side for readability. The simulation labels and conditions are summarized in Table 1. The corresponding data can be found numerically in Tables S.5–S.7 of the Supplementary Material document

a_{xy} and d_z, but are clearly distinguishable in terms of S_{chn}. Small variations of a_{xy}, d_z and S_{chn} within a given phase are due to the different CSL contents and hydration levels, to the slightly different simulation temperatures, and to the limited averaging time (statistical uncertainty).

The carbon-hydrogen order parameters $S_{\mathrm{CH}}(\mathrm{C}_n)$ of the 14 methylene groups as a function of the carbon atom number (n = 2–15) are displayed graphically at the different temperatures in Fig. 9 as calculated considering the last 24 ns of the entire set of 83 simulations. Omitting simulation $\mathrm{M_L F_{LC}}302$ (UN configurations), all the simulations can also unambiguously be classified into three distinct groups with order parameters characteristic of the ID (highest values), GL (intermediate values) or LC (low values) phase at the end of the simulation. Residual differences within a given phase are partly non-systematic, because they result from a combination of temperature effects and limited equilibration time in the given phase (which depends on the transition history of the specific simulation). There is, however, a slight tendency in the LC phase towards a decrease in the order parameters upon increasing the temperature.

Finally, the distributions of the total numbers of H-bonds per lipid ($N_{\mathrm{L}}^{\mathrm{tot}}$), per CSL ($N_{\mathrm{C}}^{\mathrm{tot}}$) and per water ($N_{\mathrm{W}}^{\mathrm{tot}}$) molecule among lipid, CSL and water partners is illustrated graphically as a function of temperature in Fig. 10, calculated considering the last 24 ns of the entire set of 83

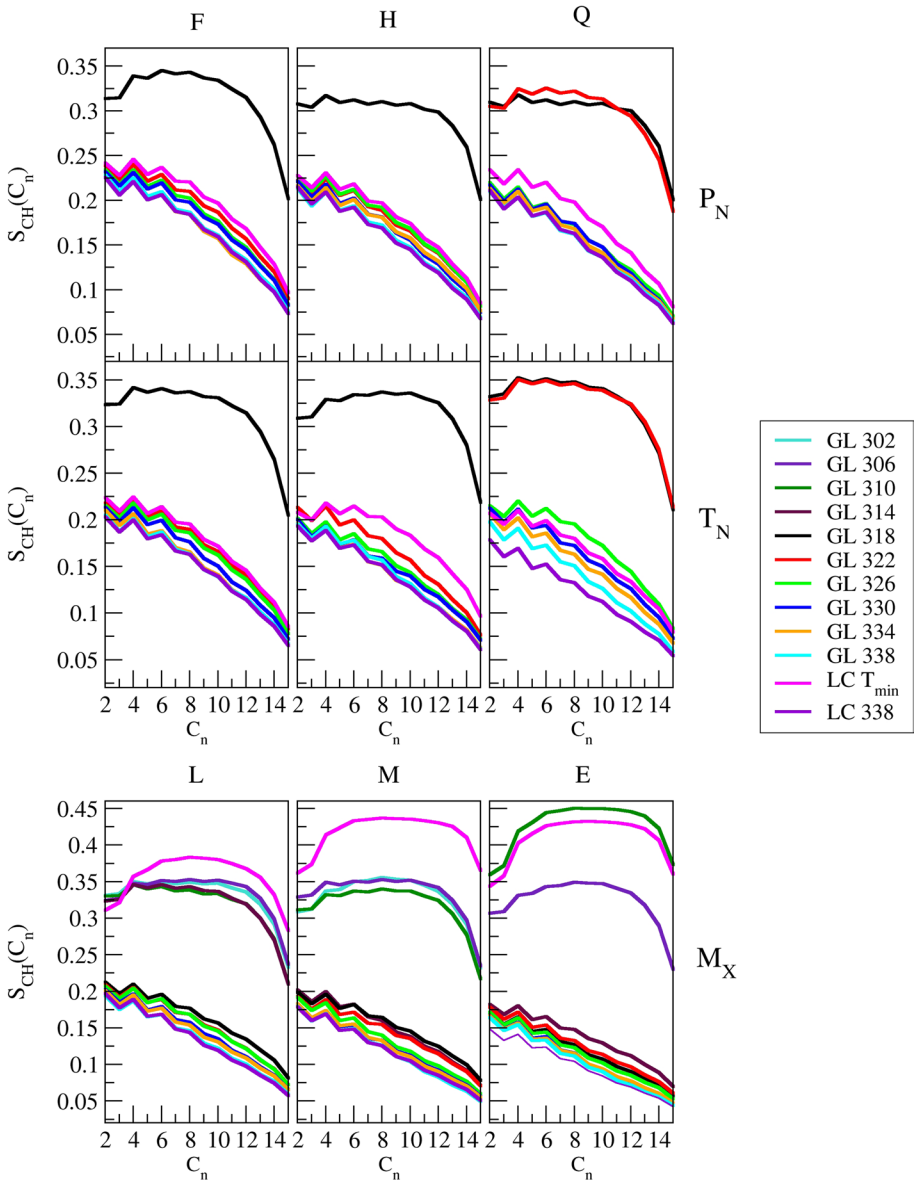

Fig. 9 Carbon-hydrogen order parameters of the 14 methylene groups for the entire set of simulations. Shown are the order parameters $S_{CH}(C_n)$ as a function of the carbon atom number C with $n = 2$–15, for the entire set of simulations. The simulations differ by the different CSLs (P, T or M), numbers of CSL molecules (N, L, M, or E) and hydration level (F, H or Q). They were started from a structure appropriate for the GL phase and carried out at reference temperatures ranging from $T_{min} = 302$ (systems M_L and M_M), 306 (system M_E) or 318 K (all other systems) to 338 K in steps of 4 K, or from a structure appropriate for the LC phase and carried out at reference temperatures T_{min} or 338 K. The data is averaged over the last 24 ns of the simulation. The simulation labels and conditions are summarized in Table 1. Note that the order parameter graphs shown in Horta et al. (2010b) (see Fig. 5 therein) and Laner et al. (2013) (see Fig. 4 therein) were affected by a small calculation error, leading to an erroneous (too low) S_{CH} (C_2) [numbered 11 in Laner et al. (2013)]

simulations. This figure generalizes the considerations on H-bond conservation made in section "Equilibrium properties" on the basis of a subset of 18 equilibrium simulations. The most striking observation is that throughout all systems considered, N_L^{tot} is always close to 4.1, N_C^{tot} close to 2.2 for MET and to 13.5 for TRH, and N_W^{tot} close to 3.2. The only factor of variability is the distribution of these H-bonds among different H-bonding partners, which is affected by the phase, CSL type and concentration, and temperature. The influence of temperature, however, is seen to be relatively weak over the range considered. The influence of the two other factors on the H-bond distributions was discussed in section "Equilibrium properties", and the corresponding considerations will not be repeated here.

Conclusion

The aim of the present study was to investigate the influence of two CSLs, TRH and MET, on the structural, dynamic and thermodynamic properties of a GMP bilayer and on its main transition temperature T_m. The main conclusions that can be drawn based on the simulation results are the following.

The LC phase is laterally expanded and transversely compact. Although it presents the largest single-lipid tilt angle, which also accounts here for chain kinks, this tilting is essentially non-collective in nature. This phase is also characterized by the lowest order parameters and the highest fluidity (lipid translational, rotational and conformational relaxation). The GL phase is the most laterally

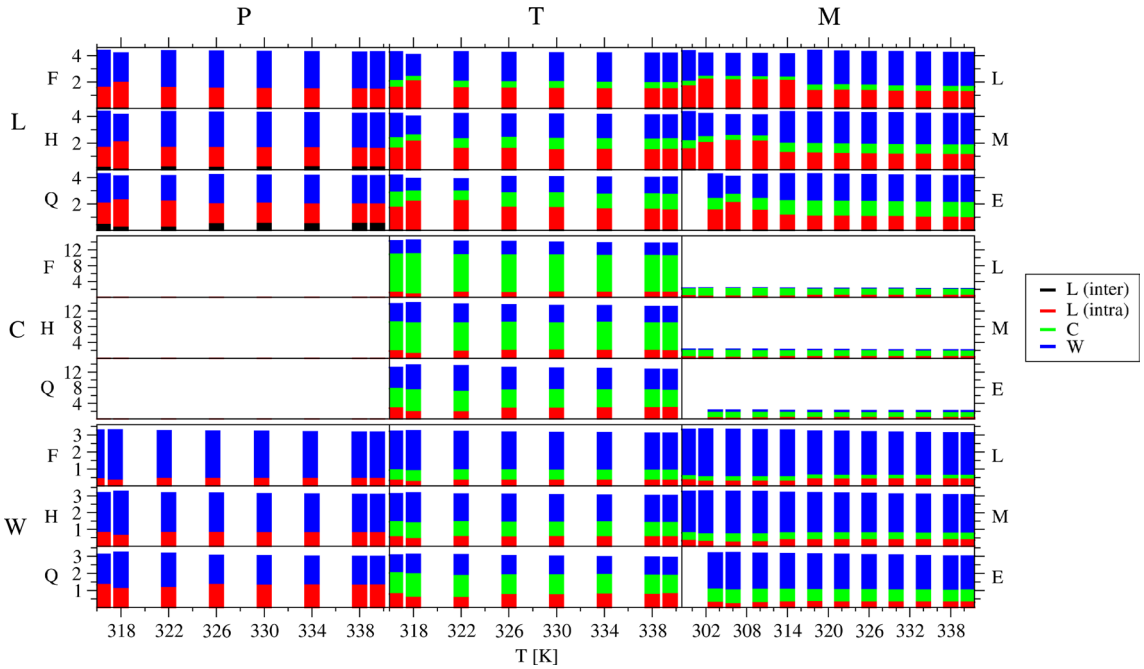

Fig. 10 Average hydrogen bonding (H-bonding) properties for the entire set of simulations. Shown are the total number of H-bonds per lipid $N_{\mathrm{L}}^{\mathrm{tot}}$ (*top panels*), per CSL $N_{\mathrm{C}}^{\mathrm{tot}}$ (*middle panels*) and per water $N_{\mathrm{W}}^{\mathrm{tot}}$ (*bottom panels*). The different colors indicate the contributions to these numbers involving lipids (inter-layer or intra-layer H-bonds distinguished for lipid-lipid H-bonds), to CSL molecules and to water molecules. The simulations differ by the different CSLs (P, T or M), numbers of CSL molecules (N, L, M, or E) and hydration level (F, H or Q). They were started from a structure appropriate for the GL phase and carried out at reference temperatures ranging from $T_{\mathrm{min}} =$ 302 (systems $\mathrm{M_L}$ and $\mathrm{M_M}$), 306 (system M*E*) or 318 K (all other systems) to 338 K in steps of 4 K, or from a structure appropriate for the LC phase and carried out at reference temperatures T_{min} or 338 K. The data is averaged over the last 24 ns of the simulation. Note that the LC *bars* were slightly shifted to the side for readability. The simulation labels and conditions are summarized in Table 1. The corresponding data can be found numerically in Tables S.8–S.10 of the Supplementary Material document

compact and transversely expanded of the three phases. Although it presents a lower single-lipid tilt angle compared to the LC phase, this tilting is almost exclusively collective in nature (value of about 20°). This phase is also characterized by higher order parameters and a reduced fluidity compared to the LC phase. Finally, the ID phase is characterized by the interdigitation of the tails from the opposite leaflets. It has a lateral expansion comparable to the LC phase, but is the transversely most compact of the three phases. The interdigitated chains are nearly aligned with the bilayer normal. This phase is characterized by the highest order parameters, resulting from both a high chain ordering (predominantly all-*trans* conformations) and the absence of a significant tilt, and by a limited fluidity comparable to that of the GL phase. The structural parameters of the GL phase are largely insensitive to the environmental conditions (hydration, presence of CSL, temperature). However, dehydration or addition of a CSL promote a lateral expansion in the LC phase. This expansion is concentration-independent for TRH, but increases with concentration for MET.

Owing to their large sizes, the molecules of TRH do not penetrate the bilayer very deeply, forming a coating layer at the bilayer surface that preserves water molecules interacting with the lipids. And due to their large numbers of potentially H-bonding groups, they induce the formation of H-bonded network bridging the lipid headgroups. Formation of a coating layer and lipid bridging may each play a role in the stabilization of the LC phase in low-hydration situations characteristic of anhydrobiosis, i.e., they may explain the suppression by TRH of the dehydration-induced T_m increase observed in pure bilayers. Owing to their small sizes and lower polarity compared to water, the molecules of MET penetrate more deeply into the bilayer surface, with the ability to intercalate between the lipids. Considering the larger volume of the MET compared to the water molecule (at lower H-bonding capacity), this effect is probably responsible for the concentration-dependent lateral expansion of the bilayer observed in the LC phase. In turn, lateral expansion may play a role in the alteration of the function of membrane-bound proteins in situations characteristic of anesthesia by alcohols. The occurrence of an ID phase may be viewed as an extreme consequence of this lateral expansion. When the expansion is important enough, the void spaces within the bilayer interior can be removed through interdigitation of the lipid tails.

Simultaneously, interdigitation induces the removal of the single-lipid tilting, and an ordering and close-packing of the chains comparable to (or higher than) those in the GL phase. The above observations are key features of what has been referred to in previous work as the sugar-like (TRH) and the alcohol-like (MET) mechanisms for the interaction of polyhydroxylated compounds with lipid bilayers (Pereira and Hünenberger 2008a).

Another fundamental difference between TRH and MET revealed by the simulations is that the former compound does not significantly affect the melting temperature of the bilayer in the concentration range considered, whereas MET appears to decrease T_m in a concentration-dependent fashion.

In principle, lowering the hydration of a pure bilayer below the full-hydration regime should lead to a T_m increase. One of the reasons invoked to explain the bioprotection effect of TRH in the context of anhydrobiosis is that this compound suppresses this T_m increase at low hydration. Although the present simulations suggest a slightly lower T_m at quarter compared to full and half hydration, they fail to evidence any influence of TRH on this behavior. However, the absence of an apparent effect may result from: (1) the relatively low concentrations of TRH in the simulated systems compared to those considered in experiments or involved in anhydrobiotic organisms; (2) the possibility that the action of TRH on GMP differs from that on the lipids (typically DPPC) investigated experimentally; (3) the difficulty of determining precise T_m values based on the finite-timescale single-event bracketing approach employed here (Laner et al. 2013; Laner and Hünenberger 2014b).

In principle, a T_m decrease with increasing MET concentration and the occurrence of a thermodynamically stable GL phase should be observed at concentrations lower than that of the biphasic reversal. Above this concentration, T_m should increase again with MET concentration, with a thermodynamically stable ID phase. Here, the picture delivered by the simulations is not entirely clear, considering that: (1) the concentration range probed in the simulations is likely above the experimental biphasic reversal concentration; (2) the simulations at the lowest temperatures lead to the occurrence of an ID rather than a GL phase; (3) the ID phase is only reached in the present simulations from the LC phase, never directly from the GL phase, suggesting a possible metastability (kinetic trapping) of the GL phase on the simulation timescale. In addition, the GL phase is metastable by nature for GMP-water systems. It has a considerable lifetime, but shows a spontaneous transition to the coagel phase (i.e., a mixture of crystals in water) (Cassin et al. 1998; Chupin et al. 2001; Sein et al. 2002; van Duynhoven et al. 2005; Horta and Hünenberger 2011). A more detailed discussion of the issues based on additional simulations is the scope of a companion article (Laner and Hünenberger 2014a).

Finally, the entire set of 83 simulations suggests the tentative formulation of two basic conservation principles, which will be called here the H-bond saturation and the densest packing principles. These principles result from the consideration that the formation of H-bonds at the bilayer surface and in solution, as well as the tail packing in the bilayer interior, are very strong driving forces, so that their optimal realization (H-bond saturation, densest packing) is a near constraint for bilayer systems at equilibrium.

The H-bond saturation principle rests on the observation that for all the species present in the different systems, the total numbers of H-bonds per molecule is essentially constant throughout the 83 simulations. This conservation actually also extends to the number of lipid-lipid H-bonds in pure GMP crystals. The only factor of variability is the distribution of these H-bonds among different H-bonding partners, which is affected by the phase, CSL type and concentration, and, more weakly, by temperature. Considering the lipids, such a nearly quantitative compensation effect between changes in the numbers of lipid-lipid and lipid-environment H-bonds upon altering the phase or environment of a bilayer, i.e., the conservation of the headgroup H-bond saturation, has been observed previously for this system (Horta et al. 2010b; Laner et al. 2013), as well as in different contexts (Pereira et al. 2004; Pereira and Hünenberger 2006, 2008a, b).

The densest packing principle rests on the observation that the effective volume per methylene group in the bilayer interior is only weakly sensitive to the environmental conditions, with values of about 0.030 (LC), 0.028 (GL) and 0.025 (ID) nm^3 for GMP based on the present simulations. These values can be compared with experimental estimates of 0.030 and 0.025 nm^3 for liquid and solid alkanes, respectively. Within the densest packing principle, these differences are neglected, and the volume per methylene group is assumed to be constant. As a result, there exists a strong correlation between the area per lipid, sensitive to the phase and environmental conditions, and most of the other structural parameters of the bilayer. For example, irrespective of the phase and environment, an increase in the area per lipid will lead to a decrease in the bilayer thickness, an increase in the single-lipid tilt angle, and a decrease in the order parameters (when interdigitation occurs, the correlation should involve the half area per lipid for the two latter observables). The collective tilt angle escapes this correlation (depending directly on the phase, not via the area per lipid) because, within the densest packing principle, the collectiveness of the single-lipid tilting does not affect the chain packing density.

According to the densest packing principle, the organization of the lipids in the bilayer under specific environmental

conditions is constrained to achieve a quasi-optimal packing of the tails given an area per lipid determined by the environmental conditions and a fixed volume per methylene group. In general, the environmentally modulated effective headgroup cross-section will be larger than the (fixed) tail cross-section, making a vertical packing of all-*trans* chains extremely unfavorable. In the context of monoglycerides, there are three possible mechanisms to relieve the effect of this mismatch between headgroup and tail cross-sections (Laner et al. 2014): (1) single-lipid tilting or kinking; (2) collective tilting; (3) interdigitation. These three mechanisms are active in the LC, GL and ID phases, respectively. For more complex lipids such as DPPC, additional mechanisms, such as glycerol backbone tilting or modulation of the packing mode of the headgroup substituents, become accessible.

The densest packing principle itself does not distinguish between single-lipid and collective tilting, which are assumed to correspond to the same packing densities. The preference for one or the other mechanism (phase) can be viewed as a temperature-dependent compromise between (for example, for a GL→LC transition): (1) the entropy increase resulting from randomizing the chain orientations and enhancing the conformational freedom of the tails; (2) the enthalpy increase resulting from slightly decreasing the packing density (deviation from the densest packing principle; the volume per methylene group actually increases by about 7 %). This temperature-dependent enthalpy-entropy balance is actually the same as that determining the melting of alkanes. In addition, the densest packing principle explains why the ID phase only occurs under environmental conditions promoting a particularly large area per lipid, such as the addition of alcohols at high concentrations. Interdigitation only becomes possible when the environmentally modulated effective headgroup cross-section is at least twice as large as the effective tail cross-section. When the ratio is exactly two, the occurrence of a non-tilted ID phase becomes possible. This is essentially the situation observed in the present simulations. If the ratio were larger than two, the formation of a tilted ID phase could also be envisioned.

Acknowledgments Financial support from the Swiss National Foundation (Grants 21-132739 and 21-138020) is gratefully acknowledged.

References

Adams DR, Toner M, Langer R (2007) Role of trehalose in prevention of giant vesicle adsorption and encapsulated solute leakage in anhydrobiotic preservation. Langmuir 23:13013–13023

Alberola C, Blümich B, Emeis D, Wittern K-P (2006) Phase transitions of monoglyceride emulsifier systems and pearlescent effects in cosmetic creams studied by ^{13}C NMR spectroscopy and DSC. Colloids Surf A Physicochem Eng Aspects 290:247–255

Albertorio F, Chapa VA, Chen X, Diaz AJ, Cremer PS (2007) The α,α-(1→1) linkage of trehalose is key to anhydrobiotic preservation. J Am Chem Soc 129:10567–10574

Anézo C, de Vries AH, Höltje H-D, Tieleman DP, Marrink S-J (2003) Methodological issues in lipid bilayer simulations. J Phys Chem B 107:9424–9433

Ariga K, Nakanishi T, Kawanami S-I, Kosaka T, Kikuchi J-I (2006) Remarkable difference of phase transition behaviors between langmuir monolayers and aqueous bilayer vesicles of oligopeptide-carrying lipids. J Nanosci Nanotechnol 6:1718–1730

Armen RD, Uitto OD, Feller SE (1998) Phospholipid component volumes: determination and application to bilayer structure calculations. Biophys J 75:734–744

Barchfeld GL, Deamer DW (1988) Alcohol effects on lipid bilayer permeability to protons and potassium: relation to the action of general anesthetics. Biochim Biophys Acta 944:40–48

Barker JA, Watts RO (1973) Monte Carlo studies of the dielectric properties of water-like models. Mol Phys 26:789–792

Baştuğ T, Patra SM, Kuyucak S (2006) Finite system and periodicity effects in free energy simulations of membrane proteins. Chem Phys Lett 425:320–323

Belton PS, Gil AM (1994) IR and Raman spectroscopic studies on the interaction of trehalose with hen egg white lysozyme. Biopolymers 34:957–961

Bennett WFD, MacCallum JL, Hinner MJ, Marrink SJ, Tieleman DP (2009) Molecular view of cholesterol flip-flop and chemical potential in different membrane environments. J Am Chem Soc 131:12714–12720

Berendsen HJC, Postma JPM, van Gunsteren WF, Hermans J (1981) Interaction models for water in relation to protein hydration. In: Pullman B (ed) Intermol Forces. Reidel, Dordrecht, pp 331–342

Berendsen HJC, Postma JPM, van Gunsteren WF, di Nola A, Haak JR (1984) Molecular dynamics with coupling to an external bath. J Chem Phys 81:3684–3690

Boggs JM, Rangaraj G (1985) Phase transitions and fatty acid spin label behavior in interdigitated lipid phases induced by glycerol and polymyxin. Biochim Biophys Acta 816:221–233

Cantor RS (1997) The lateral pressure profile in membranes: a physical mechanism of general anesthesia. Biochemistry 36:2339–2344

Cantor RS (2001) Breaking the Meyer–Overton rule: predicted effects of varying stiffness and interfacial activity on the intrinsic potency of anesthetics. Biophys J 80:2284–2297

Cassin G, de Costa C, van Duynhoven JPM, Agterof WGM (1998) Investigation of the gel to coagel phase transition in monoglyceride-water systems. Langmuir 14:5757–5763

Castro V, Stevenson B, Dvinskikh SV, Högberg K-J, Lyubartsev AP, Zimmermann H, Sandström D, Maliniak A (2008) NMR investigations of interactions between anesthetics and lipid bilayers. Biochim Biophys Acta 1778:2604–2611

Chanda J, Bandyopadhyay S (2006) Perturbation of phospholipid bilayer properties by ethanol at a high concentration. Langmuir 22:3775–3781

Chau P-L (2010) New insights into the molecular mechanisms of general anesthetics. Br J Pharmacol 161:288–307

Chen C-H, Hoye K, Roth LG (1996) Thermodynamic and fluorescence studies of the underlying factors in benzyl alcohol-induced lipid interdigitated phase. Arch Biochem Biophys 333:401–406

Chen R, Poger D, Mark AE (2011) Effect of high pressure on fully hydrated DPPC and POPC bilayers. J Phys Chem B 115:1038–1044

Chiou J-S, Krishna PR, Kamaya H, Ueda I (1992) Alcohols dehydrate lipid membranes: an infrared study on hydrogen bonding. Biochim Biophys Acta 1110:225–233

Choutko A, van Gunsteren WF, Hünenberger PH (2012) Preferential affinity of the components of liquid mixtures at a rigid nonpolar surface: enthalpic and entropic driving forces. Chem Phys Chem 12:3214–3223

Chupin V, Boots J-WP, Killian JA, Demel RA, de Kruijff B (2001) Lipid organization and dynamics of the monostearoylglycerol-water system. A 2H NMR study. Chem Phys Lipids 109:15–28

Clegg JSC (2001) A peculiar state of biological organization. Comput Biochem Physiol B 128:613–624

Cooper GM, Hausman RE (2007) The cell: a molecular approach. ASM Press, Washington

Cordomí A, Edholm O, Perez J (2007) Effect of different treatments of long-range interactions and sampling conditions in molecular dynamic simulations of rhodopsin embedded in a dipalmitoyl phosphatidylcholine bilayer. J Comput Chem 28:1017–1030

Crowe JH, Crowe LM, Chapman D (1984) Preservation of membranes in anhydrobiotic organisms: the role of trehalose. Science 223:701–703

Crowe JH, Crowe LM, Carpenter JF, Wistrom CA (1987) Stabilization of dry phospholipid bilayers and proteins by sugars. Biochem J 242:1–10

Crowe JH, Hoekstra FA, Crowe LM (1992) Anhydrobiosis. Annu Rev Physiol 54:579–599

Crowe JH, Carpenter JF, Crowe LM (1998) The role of vitrification in anhydrobiosis. Annu Rev Physiol 60:73–103

Crowe LM (2002) Lessons from nature: the role of sugars in anhydrobiosis. Comp Biochem Physiol 131A:505–513

Crowe JH, Oliver AE, Tablin F (2002) Is there a single biochemical adaptation to anhydrobiosis? Integr Comput Biol 42:497–503

Crowe JH, Crowe LM, Wolkers WF, Oliver AE, Ma X, Auh J-H, Tang M, Zhu S, Norris J, Tablin F (2005) Stabilization of dry mammalian cells: lessons from nature. Integr Comp Biol 45:810–820

de Vries AH, Yefimov S, Mark AE, Marrink SJ (2005a) Molecular structure of the lecithin ripple phase. Proc Natl Acad Sci 102:5392–5396

de Vries AH, Chandrasekhar I, van Gunsteren WF, Hünenberger PH (2005b) Molecular dynamics simulations of phospholipid bilayers: influence of artificial periodicity, system size, and simulation time. J Phys Chem 109:11643–11653

Douliez J-P, Ferrarini A, Dufourc E-J (1998) On the relationship between C-C and C-D order parameters and its use for studying the conformation of lipid acyl chains in biomembranes. J Chem Phys 109:2513–2518

Fang Z, Ionescu P, Chortkoff BS, Kandel L, Sonner J, Laster MJ, Eger E (1997) Anesthetic potencies of *n*-alkanols: results of additivity and solubility studies suggest a mechanism of action similar to that for conventional inhaled anesthetics. Anesth Analg 84:1042–1048

Feovilova EP (2003) Deceleration of vital activity as a universal biochemical mechanism ensuring adaptation of microorganisms to stress factors: a review. Appl Biochem Microbiol 39:1–18

Foubert I, Dewettinck K, van de Walle D, Dijkstra AJ, Quinn PJ (2007) Physical properties: structural and physical characteristics. In: Gunstone FD, Harwood JL, Dijkstra AJ (eds) The lipid handbook, 3rd edn. CRC Press, Division of Taylor, Francis Group, Boca Raton, USA, pp 471–534

Franks NP (2006) Molecular targets underlying general anaesthesia. Br J Pharmacol 147:72–81

Franks NP (2008) General anaesthesia: from molecular targets to neuronal pathways of sleep and arousal. Nat Rev Neurosci 9:370–386

Geerke DP, van Gunsteren WF, Hünenberger PH (2010) Molecular dynamics simulations of the interaction between polyhydroxylated compounds and Lennard-Jones walls: preferential affinity/exclusion effects and their relevance for bioprotection. Mol Simul 36:708–728

Goto M, Takiguchi T (1985) The crystal structure of the β-form of α-monolaurin. Bull Chem Soc Jpn 58:1319–1320

Goto M, Kozo K, Uchida T (1988) The crystal structure of the β_1' form of optically active α-monostearin. Bull Chem Soc Jpn 61:1434–1436

Green JL, Angell CA (1989) Phase relations and vitrification in saccharide-water solutions and the trehalose anomaly. J Phys Chem 93:2880–2882

Griffin KL, Cheng C-Y, Smith EA, Dea P (2010) Effects of pentanol isomers on the phase behavior of phospholipid bilayer membranes. Biophys Chem 152:178–183

Guppy M, Withers P (1999) Metabolic depression in animals: physiological perspectives and biochemical generalizations. Biol Rev 74:1–40

Gurtovenko AA, Anwar J (2009) Interaction of ethanol with biological membranes: the formation of non-bilayer structures within the membrane interior and their significance. J Phys Chem B 113:1983–1992

Hargreaves WR, Mulvihill SJ, Deamer (1976) Synthesis of phospholipids and membranes in perbiotic conditions. Nature 3:78–80

Heinz TN, van Gunsteren WF, Hünenberger PH (2001) Comparison of four methods to compute the dielectric permittivity of liquids from molecular dynamics simulations. J Chem Phys 115:1125–1136

Hengherr S, Heyer AG, Koehler H, Schill R (2008) Trehalose and anhydrobiosis in tardigrades—evidence for divergence in responses to dehydration. FEBS J 275:281–288

Herce DH, Garcia AE (2006) Correction of apparent finite size effects in the area per lipid of lipid membranes simulations. J Chem Phys 125:224711/1–224711/13

Hicke L, Dunn R (2003) Regulation of membrane protein transport by ubiquitin and ubiquitin-binding proteins. Annu Rev Cell Dev Biol 19:141–172

Hincha DK, Zuther E, Hellwege EM, Heyer AG (2002) Specific effects of fructo- and gluco-oligosaccharides in the preservation of liposomes during drying. Glycobiology 12:103–110

Hincha DK, Hagemann M (2004) Stabilization of model membranes during drying by compatible solutes involved in the stress tolerance of plants and microorganisms. Biochem J 383:277–283

Hockney RW (1970) The potential calculation and some applications. Methods Comput Phys 9:136–211

Hoekstra FA, Golovina EA, Buitink J (2001) Mechanisms of plant desiccation tolerance. J Trends Plant Sci 6:431–438

Holte LL, Gawrisch K (1997) Determining ethanol distribution in phospholipid multilayers with MAS-NOESY spectra. Biochemistry 36:4669–4674

Horta BAC, Perić-Hassler L, Hünenberger PH (2010a) Interaction of the disaccharides trehalose and gentiobiose with lipid bilayers: a comparative molecular dynamics study. J Mol Graph Model 29:331–346

Horta BAC, de Vries AH, Hünenberger PH (2010b) Simulating the transition between gel and liquid-crystal phases of lipid bilayers: dependence of the transition temperature on the hydration level. J Chem Theory Comput 6:2488–2500

Horta BAC, Fuchs PFJ, van Gunsteren WF, Hünenberger PH (2011) New interaction parameters for oxygen compounds in the GROMOS force field: improved pure-liquid and solvation properties for alcohols, ethers, aldehydes, ketones, carboxylic acids and esters. J Chem Theory Comput 7:1016–1031

Horta BAC, Hünenberger PH (2011) Enantiomeric segregation in the gel phase of lipid bilayers. J Am Chem Soc 133:8464–8466

Kastenholz MA, Hünenberger PH (2004) Influence of artificial periodicity and ionic strength in molecular dynamics simulations of charged biomolecules employing lattice-sum methods. J Phys Chem B 108:774–788

Katsaras J, Yang DSC, Epand RM (1992) Fatty-acid chain tilt angles and directions in dipalmitoyl phosphatidylcholine bilayers. Biophys J 63:1170–1175

Keilin D (1959) The Leeuwenhoek lecture: The problem of anabiosis or latent life—history and current concept. Proc R Soc Lond B Biol Sci 150:149–191

Klauda JB, Brooks BR, Pastor RW (2006) Dynamical motions of lipids and a finite size effect in simulations of bilayers. J Chem Phys 125:144710/1–144710/8

Klauda JB, Venable RM, MacKerell AD Jr, Pastor RW (2008) Considerations for lipid force field development. Curr Top Membr 60:1–48

Knecht V, Marrink S-J (2007) Molecular dynamics simulations of lipid vesicle fusion in atomic detail. Biophys J 92:4254–4261

Koenig BW, Gawrisch K (2005) Specific volumes of unsaturated phosphatidylcholines in the liquid crystalline lamellar phase. Biochim Biophys Acta 1715:65–70

Koster KL, Webb MS, Bryant G, Lynch DV (1994) Interactions between soluble sugars and POPC (1-palmitoyl-2-oleoylphosphatidylcholine) during dehydration: vitrification of sugars alters the phase behavior of the phospholipid. Biochim Biophys Acta 1193:143–150

Kranenburg M, Vlaar M, Smit B (2004) Simulating induced interdigitation in membranes. Biophys J 87:1596–1605

Kristiansen K (2004) Molecular mechanisms of ligand binding, signaling, and regulation within the superfamily of G-protein-coupled receptors: Molecular modeling and mutagenesis approaches to receptor structure and function. Pharmacol Therap 103:21–80

Krog N, Larsson K (1968) Phase behaviour and rheological properties of aqueous systems of industrial distilled monoglycerides. Chem Phys Lipids 2:129–143

Krog N, Borup AP (1973) Swelling behaviour of lamellar phases of saturated monoglycerides in aqueous systems. J Sci Food Agric 24:691–701

Kulkarni K, Snyder DS, McIntosh TJ (1999) Adhesion between cerebroside bilayers. Biochemistry 38:15264–15271

Kunz A-PE, Allison JR, Geerke DP, Horta BAC, Hünenberger PH, Riniker S, Schmid N, van Gunsteren WF (2012) New functionalities in the GROMOS biomolecular simulation software. J Comput Chem 33:340–353

Kurniawan Y, Venkataramanan KP, Scholz C, Bothun GD (2012) *n* -butanol partitioning and phase behavior in DPPC/DOPC membranes. J Phys Chem B 116:5919–5924

Laner M, Horta BAC, Hünenberger PH (2013) Phase-transition properties of glycerol-monopalmitate lipid bilayers investigated by molecular dynamics simulation: influence of the system size and force-field parameters. Mol Simul 39:563–583

Laner M, Horta BAC, Hünenberger PH (2014) Long-timescale motions in glycerol-monopalmitate lipid bilayers investigated using molecular dynamics simulation. J Mol Graph Model (submitted)

Laner M, Hünenberger PH (2014a) Effect of methanol on the phase-transition properties of glycerol-monopalmitate lipid bilayers investigated using molecular dynamics simulations: in quest of the biphasic effect. J Mol Graph Model (submitted)

Laner M, Hünenberger PH (2014b) Thermodynamics and kinetics of the gel to liquid-crystal phase transitions in glycerol-monopalmitate lipid bilayers: a Markov model analysis based on atomistic molecular dynamics simulations. To be submitted

Larsson K (1966) The crystal structure of the L-1-monoglyceride of 11-bromoundecanoic acid. Acta Crystallogr 21:267–272

Lee BW, Faller R, Sum AK, Vattulainen I, Patra M, Karttunen M (2004) Structural effects of small molecules on phospholipid bilayers investigated by molecular simulations. Fluid Phase Equilib 225:63–68

Lee BW, Faller R, Sum AK, Vattulainen I, Patra M, Karttunen M (2005) Structural effects of small molecules on phospholipid bilayers inverstigated by molecular simulations. Fluid Phase Equilib 228:135–140

Lenné T, Garvey CJ, Koster KL, Bryant G (2009) Effects of sugars on lipid bilayer during dehydration—SAXS/WAXS measurement and quantitative model. J Phys Chem B 113:2486–2491

Lindahl E, Edholm O (2000) Spatial and energetic-entropic decomposition of surface tension in lipid bilayers from molecular dynamics simulations. J Chem Phys 113:3882–3893

Lins RD, Pereira SC, Hünenberger PH (2004) Trehalose-protein interaction in aqueous solution. Proteins Struct Funct Bioinform 55:177–186

Lins RD, Hünenberger PH (2005) A new GROMOS force field for hexopyranose-based carbohydrates. J Comput Chem 26:1400–1412

Löbbecke L, Cevc G (1995) Effects of short-chain alcohols on the phase behavior and interdigitation of phosphatidylcholine bilayer membranes. Biochim Biophys Acta 1237:59–69

Ly HV, Longo ML (2004) The influence of short-chain alcohols on interfacial tension, mechanical properties, area/molecule, and permeability of fluid lipid bilayers. Biophys J 87:1013–1033

Lyubartsev AP, Rabinovich AL (2011) Recent development in computer simulation of lipid bilayers. Soft Matter 7:25–39

MacCallum JL, Tieleman DP (2008) Interactions between small molecules and lipid bilayers. Curr Top Membr 60:227–256

Marrink S-J, Berger O, Tieleman P, Jähnig F (1998) Adhesion forces of lipids in a phospholipid membrane studied by molecular dynamics simulations. Biophys J 74:931–943

McIntosh TJ (2000) Short-range interactions between lipid bilayers measured by X-ray diffraction. Curr Opin Struct Biol 10:481–485

Miyamoto S, Kollman PA (1992) SETTLE : an analytical version of the SHAKE and RATTLE algorithm for rigid water models. J Comput Chem 13:952–962

Morley WG, Tiddy GJT (1993) Phase behavior of monoglyceride/water systems. J Chem Soc Faraday Trans 89:2823–2831

Mou J, Yang J, Huang C, Shao Z (1994) Alcohol induces interdigitated domains in unilamellar phosphatidylcholine bilayers. Biochemistry 33:9981–9985

Nagarajan S, Schuler EE, Ma K, Kindt JT, Dyer RB (2012) Dynamics of the gel to fluid phase transformation in unilamellar DPPC vesicles. J Phys Chem B 116:13749–13756

Nagle JF, Wiener MC (1988) Structure of fully hydrated bilayer dispersions. Biochim Biophys Acta 942:1–10

Nagle JF, Tristram-Nagle S (2000) Structure of lipid bilayers. Biochim Biophys Acta 1469:159–195

Nakagaki M, Nagase H, Ueda H (1992) Stabilization of the lamellar structure of phosphatidylcholine by complex formation with trehalose. J Membr Sci 73:173–180

Ohki K, Tamura K, Hatta I (1990) Ethanol induces interdigitated gel phase ($L_{\beta I}$) between lamellar gel phase ($L_{\beta'}$) and ripple phase ($P_{\beta'}$) in phosphatidylcholine membranes: A scanning density meter study. Biochim Biophys Acta 1023:215–222

Olasagasti F, Maurel M-C, Deamer DW (2014) Physico-chemical interactions between compartmentforming lipids and other prebiotically relevant biomolecules. BIO Web Conf 2:05001/1–05001/10

Oostenbrink C, Villa A, Mark AE, van Gunsteren WF (2004) A biomolecular force field based on the free enthalpy of hydration and solvation: the GROMOS force-field parameter sets 53A5 and 53A6. J Comput Chem 25:1656–1676

Patra M, Karttunen M, Hyvönen MT, Falck E, Lindqvist P, Vattulainen I (2003) Molecular dynamics simulations of lipid bilayers: major artifacts due to truncating electrostatic interactions. Biophys J 84:3636–3645

Patra M, Karttunen M, Hyvönen MT, Falck E, Vattulainen I (2004) Lipid bilayers driven to a wrong lane in molecular dynamics simulations by subtle changes in long-range electrostatic interactions. J Phys Chem B 108:4485–4494

Patra M, Salonen E, Terama E, Vattulainen I, Faller R, Lee BW, Holopainen J, Karttunen M (2006) Under the influence of alcohol: the effect of ethanol and methanol on lipid bilayers. Biophys J 90:1121–1135

Pereira CS, Lins RD, Chandrasekhar I, Freitas LCG, Hünenberger PH (2004) Interaction of the disaccharide trehalose with a phospholipid bilayer: a molecular dynamics study. Biophys J 86:2273–2285

Pereira CS, Hünenberger PH (2006) Interaction of the sugars trehalose, maltose and glucose with a phospholipid bilayer: a comparative molecular dynamics study. J Phys Chem B 110:15572–15581

Pereira CS, Hünenberger PH (2008a) The influence of polyhydroxylated compounds on a hydrated phospholipid bilayer: a molecular dynamics study. Mol Simul 34:403–420

Pereira CS, Hünenberger PH (2008b) Effect of trehalose on a phospholipid membrane under mechanical stress. Biophys J 95:3525–3534

Pezron I, Pezron E, Bergenstahl BA, Claesson PM (1990) Repulsive pressure between monoglyceride bilayers in the lamellar and gel states. J Phys Chem 94:8255–8261

Pezron I, Pezron E, Claesson PM, Bergenstahl BA (1991) Monoglyceride surface films: stability and interlayer interactions. J Coll Interface Sci 144:449–457

Pierce KL, Premont RT, Lefkowitz RJ (2002) Seven transmembrane receptors. Nat Rev Molec Cell Biol 3:639–650

Qin S-S, Yu Z-W, Yu Y-X (2009) Structural characterization on the gel to liquid-crystal phase transition of fully hydrated DSPC and DSPE bilayers. J Phys Chem B 113:8114–8123

Raviv U, Laurat P, Klein J (2001) Fluidity of water confined to subnanometre films. Nature 413:51–54

Reif MM, Kräutler V, Kastenholz MA, Daura X, Hünenberger PH (2009) Explicit-solvent molecular dynamics simulations of a reversibly-folding β-heptapeptide in methanol: influence of the treatment of long-range electrostatic interactions. J Phys Chem B 113:3112–3128

Ricker J, Tsvetkova N, Wolkers W, Leidy C, Tablin F, Longo M, Crowe J (2003) Trehalose maintains phase separation in an air-dried binary lipid mixture. Biophys J 84:3045–3051

Rosser MFN, Lu HM, Dea P (1999) Effect of alcohols on lipid bilayers with and without cholesterol: the dipalmitoylphosphatidylcholine system. Biophys Chem 81:33–44

Rowe ES (1983) Lipid chain length and temperature dependence of ethanol-phosphatidylcholine interactions. Biochemistry 22:3299–3305

Rowe ES (1985) Thermodynamic reversibility of phase transitions. Specific effects of alcohols on phosphatidylcholines. Biochim Biophys Acta 813:321–330

Rowe ES, Campion JM (1994) Alcohol induction of interdigitation in distearoylphosphatidylcholine: fluorescence studies of alcohol chain length requirements. Biophys J 67:1888–1895

Rudolph U, Antkowiak B (2004) Molecular and neuronal substrates for anaesthetics. Nat Rev Neurosci 5:709–720

Ryckaert J-P, Ciccotti G, Berendsen HJC (1977) Numerical integration of the Cartesian equations of motion of a system with constraints: molecular dynamics of *n*-alkanes. J Comput Phys 23:327–341

Saito H, Shinoda W (2011) Cholesterol effect on water permeability through DPPC and PSM lipid bilayers: a molecular dynamics study. J Phys Chem B 115:15241–15250

Schmid N, Christ CD, Christen M, Eichenberger AP, van Gunsteren WF (2012) Architecture, implementation and parallelisation of the GROMOS software for biomolecular simulation. Comput Phys Commun 183:890–903

Seddon JM, Cevc G (1993) Lipid polymorphism: structure and stability of lyotropic mesophases of phospholipids. In: Cevc G (ed) Phospholipids handbook. Marcel Dekker, INC., New York, pp 403–454

Sein A, Verheij JA, Agterof WGM (2002) Rheological characterization, crystallization, and gelation behavior of monoglyceride gels. J Colloid Interface Sci 249:412–422

Simon SA, McIntosh TJ (1984) Interdigitated hydrocarbon chain packing causes the biphasic transition behavior in lipid/alcohol suspensions. Biochim Biophys Acta 773:169–172

Skibinsky A, Venable RM, Pastor RW (2005) A molecular dynamics study of the response of lipid bilayers and monolayers to trehalose. Biophys J 89:4111–4121

Small DM (1984) Lateral chain packing in lipids and membranes. J Lip Res 25:1490–1500

Sun WQ, Leopold AC (1997) Cytoplasmic vitrification and survival of anhydrobiotic organisms—a viability equation analysis. Comp Biochem Physiol A 117:327–333

Takaoka Y, Pasenkievicz-Gierula M, Miyagawa H, Kitamura K, Tamura Y, Kusumi A (2000) Molecular dynamics generation of nonarbitrary membrane models reveals lipid orientational correlations. Biophys J 79:3118–3138

Tieleman DP, Marrink SJ, Berendsen HJC (1997) A computer perspective of membranes: molecular dynamics studies of lipid bilayers systems. Biochim Biophys Acta 1331:235–270

Tieleman DP, Hess B, Sansom MSP (2002) Analysis and evaluation of channel models: simulation of alamethicin. Biophys J 83:2393–2407

Tironi IG, Sperb R, Smith PE, van Gunsteren WF (1995) A generalized reaction field method for molecular dynamics simulations. J Chem Phys 102:5451–5459

Tsvetkova NM, Phillips BL, Crowe LM, Crowe JH, Risbud SH (1998) Effect of sugars on headgroup mobility in freeze-dried dipalmitoylphosphatidylcholine bilayers: solid-state 31P NMR and FTIR studies. Biophys J 75:2947–2955

Tunnacliffe A, de Castro AG, Manzanera M (2001) Anhydrobiotic engineering of bacterial and mammalian cells: Is intracellular trehalose sufficient? Cryobiology 43:124–132

Tunnacliffe A, Lapinski J (2003) Resurrecting van Leeuwenhoek's rotifers: a reappraisal of the role of disaccharides in anhydrobiosis. Phil Trans R Soc Lond B 358:1755–1771

Ueda I, Kamaya H (1984) Molecular mechanisms of anesthesia. Anesth Analg 63:929–945

van Duynhoven JPM, Broekmann I, Sein A, van Kempen GMP, Goudappel G-JW, Veeman WS (2005) Microstructural investigation of monoglyceride-water coagel systems by NMR and Cryo-SEM. J Colloid Interface Sci 285:703–710

van Gunsteren WF, Berendsen HJC (1990) Computer simulation of molecular dynamics: methodology, applications and perspectives in chemistry. Angew Chem Int Ed 29:992–1023

van Gunsteren WF, Billeter SR, Eising AA, Hünenberger PH, Krüger P, Mark AE, Scott WRP, Tironi IG (1996) Biomolecular simulation: the GROMOS96 manual and user guide. Verlag der Fachvereine, Zürich

van Gunsteren WF (2011) The GROMOS software for biomolecular simulation. Available at: http://www.gromos.net

Vaz WLC, Clegg RM, Hallmann D (1985) Translational diffusion of lipids in liquid-crystalline phase phosphatidylcholine multibilayers—a comparison of experiment with theory. Biochemistry 24:781–786

Venturoli M, Sperotto MM, Kranenburg M, Smit B (2006) Mesoscopic models of biological membranes. Phys Rep 437:1–54

Walser R, Mark AE, van Gunsteren WF, Lauterbach M, Wipff G (2000) The effect of force-field parameters on properties of

liquids: parametrization of a simple three-site model for methanol. J Chem Phys 112:10450–10459

Wanderlingh U, D'Angelo G, Conti Nibali V, Crupi C, Rifici S, Corsaro C, Sabatino G (2010) Interaction of alcohol with phospholipid membrane: NMR and XRD investigations on DPPC-hexanol system. Spectroscopy 24:375–380

Wang Y, Dea P (2009) Interaction of 1-propanol and 2-propanol with dipalmitoylphosphatidylcholine bilayer: a calorimetric study. J Chem Eng Data 54:1447–1451

Watanabe M (2006) Anhydrobiosis in invertebrates. Appl Entomol Zool 41:15–31

Westerman PW, Pope JM, Phonphok N, Doane JW, Dubro DW (1988) The interaction of n-alkanols with lipid bilayer membranes: a ^{2}H-NMR study. Biochim Biophys Acta 939:64–78

Westh P (2008) Glucose, sucrose and trehalose are partially excluded from the interface of hydrated DMPC bilayers. Phys Chem Chem Phys 10:4110–4112

Wright JC (2001) Cryptobiosis 300 years on from van Leeuwenhoek: What have we learned about tardigrades? Zool Anz 240:563–582

Yamamoto E, Akimoto T, Shimizu H, Hirano Y, Yasui M, Yasuoka K (2012) Diffusive nature of xenon anesthetic changes properties of a lipid bilayer: molecular dynamics simulations. J Phys Chem B 116:8989–8995

Yamazaki M, Ohshika M, Kashiwagi N, Asano T (1992) Phase transitions of phospholipid vesicles under osmotic stress and in the presence of ethylene glycol. Biophys Chem 43:29–37

Zhmakin AI (2008) Physical aspects of cryobiology. Phys Uspekhi 51:231–252